Czech Technical University in Prague
Faculty of Nuclear Sciences and Physical Engineering

Diploma Thesis

Study of Properties of b-tagged Jets.

Prague, 2010 **Author:Michal Vajzer**

zadanie

Title: Study of properties of b-tagged jets.
Author: Bc. Michal Vajzer
Specialization: Nuclear Engeneering
Sort of project: Diploma Thesis
Supervisor: Mgr. Jaroslav Bielčík, Ph.D., Katedra fyziky, FJFI, ČVUT v Praze.

Abstract:

Jets are important source of information and testing probe of predictions made by quantum chromodynamics. In RHIC experiments, they have proven to be invaluable in studies involving hot nuclear medium and, therefore, will become crucial in studies of quark-gluon plasma at energies produced by Large Hadron Collider, also called a jet factory. LHC energies will produce higher rates of rare high p_T partons, including heavy beauty quarks. These will play significant role in multiple areas of scientific search, therefore their identification is necessary. This work present study of jets containing these heavy beauty quarks in simulated proton-proton collisions at ALICE, focusing on algorithm, method, that will search and identify them. Furthermore, a glimpse on structure of these jets is given in form of jet shapes and j_T distributions of data sample.

Key words: jet reconstruction, tagging, beauty quark, collision, Pythia, AliRoot

Názov práce: Studium vlastností jetů obsahujících těžký kvark
Autor: Bc. Michal Vajzer

Abstrakt:

Jety sú dôležitým zdrojom informácii a testovacími sondami predpovedí kvantovej chromodynamiky.V experimentoch na RHIC sa ukázali byť neoceniteľné v štúdiách týkajúcich sa horúcej jadrovej hmoty, a preto budú veľmi doležité pri štúdiu kvark-gluónovej plazmy pri energiách produkovaných na LHC, taktiež zvanom továrňa na jety. Energie na LHC vyprodukujú väčšie množstvo partónov s veľkou priečnou hybnosťou aj ťažké b-kvarky. Tieto zohrajú dôležitú úlohu v niekoľkých oblastiach vedeckého bádania, preto ich identifikácia je nutná. Táto práca prezentuje štúdiu jetov obsahujúcich ťažké b-kvarky v simulovaných zrážkach protónov v ALICE, zameriavajúc sa na algoritmus, metódu, ktorá ich vyhľadá a identifikuje. Okrem toho, krátky náhľad na štruktúru týchto jetov je daný prostredníctvom tvarov jetov a j_T distribúcie vzorky dát.

Kľúčové slová: rekonštrukcia jetov, identifikácia, krásny kvark, zrážka, Pythia, AliRoot

Acknowledgment

I would like to thank my supervisor, Jaroslav Bielčík, for his patience and help during creation of this work, and Čeněk Zach for software compilation and downloading of data from GRID. Last but not least, my thanks belongs to my family for their support up until now.

Prehlásenie

Prehlasujem, že som svoju diplomovú prácu vypracoval samostatne a použil som iba podklady (literatúru, projekty, SW atd.) uvedené v priloženom zozname.

Nemám závažný dôvod proti použitiu tohto školského diela v zmysle §60 Zákona č.121/2000 Sb., o práve autorskom, o právach súvisiacich s právom autorským a o zmene niektorých zákonov (autorský zákon).

V Prahe dňa 5. mája 2010

podpis

Table of Contents

List of Figures

List of Tables

Introduction

During recent years, it is possible to produce hot and dense nuclear matter in heavy ion collisions at experiments in CERN and BNL. New state of matter, with quarks and gluons as main degree of freedom, was produced and studied.Plenty of experimental observables was used to extract properties of produced matter. Measuring the jet production is one of them.

Jets in general play important role in physics, as observables of quantum chromodynamics. In this work, jets produced from beauty quarks are studied. The algorithm for their reconstruction is proposed.

In the first chapter, algorithms used to reconstruct and study jets are presented, namely FastJet and SISCone algorithms. Additionally, methods of tagging heavy flavour in general are described there.

Second chapter deals with ALICE experiment, with description of detectors in central region that are used for track reconstruction and identification, these being described as well. Subsequently, first results produced by ALICE, LHC's status and plans for future are mentioned.

In the Chapter 3, the analysis of simulated data containing beauty quarks is discussed in detail. The methods to reconstruct jets and identify the b-jets are described. Several properties of jets are extracted as well.

Chapter 1

Jets and beauty tagging

In this chapter, I will discuss methods used for reconstruction of jets containing beauty quark. First of all, I will cover topic of different jet algorithms, afterwards I will proceed to tagging of beauty quarks in events.

1.1 Beauty jets

Jets,observables of quantum chromodynamics, are collimated hadrons produced along quarks and gluons in their final state. These quarks and gluons are produced by hard scattering in collision of protons and heavy ion nuclei at high energies. Study of jet spectra allows study of quark composition to a distances smaller than atto-metres and precise measurements of jet's internal structure enables study of fragmentation of quarks and gluons of the jet. Furthermore, jets may replace particles in, for example, search for W or Z, whose possible decay channels include these jets.

From RHIC, Relativistic Heavy Ion Collider, energies on, jets may be used to study dense quark-gluon plasma and nuclear medium produced in collision of heavy ions as rate of rare high- p_T partons becomes high enough. It has been shown that production of jets is suppressed in collisions where partons they have to travel significant distances through dense fireball. This has been observed from azimuthal correlations of particles with high-p_T, where peak is observed at near-side, but away-side peak diminishes in central collisions of gold ions. Interpretation of these data is such that high-p_T trigger hadron identifies jet moving from fireball, but this represents only jets going from a thin surface layer, as fast partons travelling through fireball lose energy and therefore no jet is observed on the other side of fireball, associated to parton created in pair with parton, from hard scattering, whose jet is observed.

For LHC, Large Hadron Collider, higher expected energies suggest hotter medium and more high-p_T partons produced to test it, also higher rates of heavy-flavoured quarks is expected. They enable detailed studies of production mechanisms and test quantum chromodynamics. Heavy quarks have been proposed as good probes of quark-gluon plasma, because they have smaller formation time than expected formation time of quark-gluon plasma. Moreover, heavier the quark is, more significant is so-called dead-cone effect, effect of suppressed gluon radiation into small angles, leading to relative energy loss in case of heavy-flavour quarks is smaller than relative energy loss in case of light quarks.

1.2 Jet algorithms

There are two main types of algorithms to reconstruct the jet, i.e. cone and recombination algorithms. Because reconstructed jets are in fact collimated particles moving in roughly same direction, to extract and study physical properties and values, these algorithms should ensure infra-red and collinear safety. This means that addition of collinear or infra-red particle into jet shall not change extracted properties and values.

Infra-red safe algorithms, as seen in Fig. 1.1a, reconstructs jets in such a way, that when soft particle is radiated between these jets, it does not change result of reconstruction. In case of collinear safety, reconstruction algorithm is collinear safe when reconstructed result does not differ in case of energy being distributed into adjacent detector towers, as seen in Fig. 1.1b. Another case of collinear safety is sensitivity to energy ordering, as seen in Fig. 1.1c, where distribution of energy of one tower to several adjacent detector towers, changes direction, area and total energy of reconstructed jet, because energetic towers at the border of original jet may not be included in newly reconstructed one.

With these algorithms, we are trying to reconstruct direction of original jet, its energy and end energy distribution within jet.

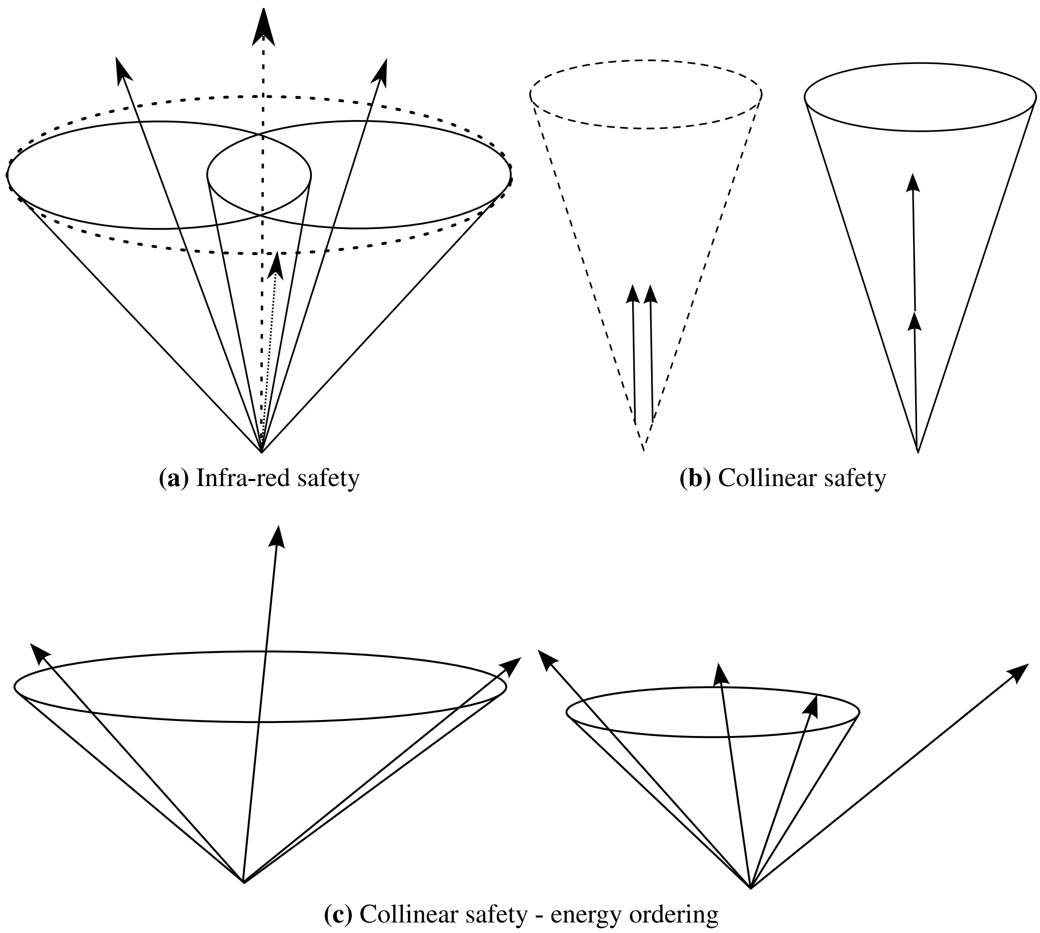

Figure 1.1: Illustration of infra-red and collinear safety, where arrows indicate particles creating jets, indicated by circle.

1.2.1 Cone algorithms

Idea behind cone algorithm is identification of energy flow into cone in phase-space given by azimuthal angle (ϕ) and rapidity (y) or pseudo-rapidity (η). It may be done in several iterations, where splitting and merging should be dealt with. Majority of cone algorithm is infra-red and/or collinear unsafe and most time-consuming part of algorithm is finding of stable jets. In Fig. 1.2, there are particles in $\eta-\phi$ phase-space, with reconstructed cone jets inside circles draw around particles creating them.

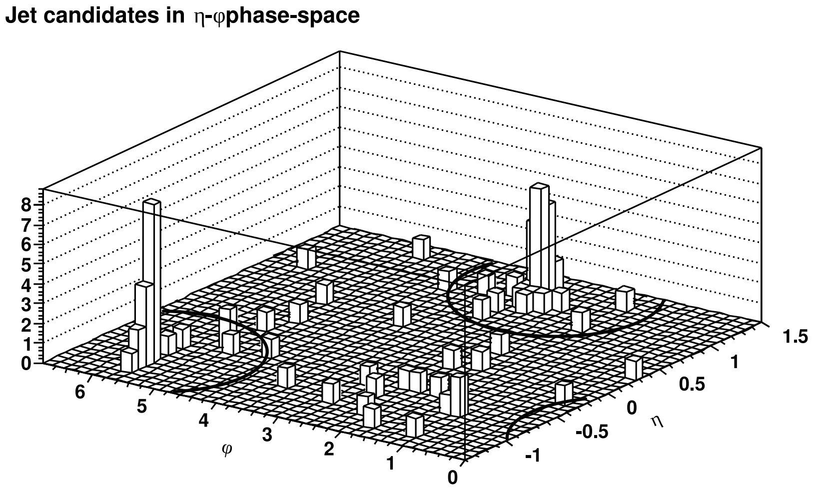

Figure 1.2: Cones of reconstructed jets from particles in $\eta - \phi$ phase-space.

This type of algorithm is based on UA1 jet-finding algorithm and may be with seeds or may be seedless, i.e. it may or may not search through $\eta - \phi$ phase-space for particles or detector towers with sufficient momentum or energy, which may be used as seed, starting point of jet-finder, around which jet-cone is searched for.

SISCone algorithm

Example of cone algorithm that is used nowadays is SISCone, i.e. Seedless Infrared Safe Cone algorithm, developed by Gavin Salam and Gregory Soyez, [19].

Scheme of this algorithm is as follows:

1. Put set of 'current particles' equal to set of all particles in the event.
2. Find all stable cones for set of 'current particles'.
3. Add each stable cone to list of protojets.
4. Remove all particles that are used in stable cones from set of 'current particles'.
5. If no new stable cone is fount or number of loops has reached preset number continue, else go to first item.

6. Run split/merge procedure on list of protojets with overlap fraction f, i.e. minimum fraction of energy shared between two protojets to merge them.

Algorithm for determination of stable cones is as follows:

1. Set particle i as first particle.

2. Find all particles j within $2R$[1] radius and for each j define two circles defined by i and j. For each circle compute angle between its centre C relative to particle i ($\zeta = \arctan(\frac{d\phi_{iC}}{dy_{iC}})$).

3. Sort circles in increasing ζ.

4. For first circle in this order calculate total momentum and check for the cones that it defines. Consider all permutation of particles on edge being included or excluded.Call these 'current cones'.

5. For each of 'current cones',

   - If this cone has not been fount, add it to list of 'distinct cones'.
   - If cone has not been labelled unstable, define it's stability using particles at the edge of cone.

6. Move to next circle in order. If it differs from previous one, with respect to its particle content, calculate momentum of new circle.

7. For all cones not labelled as unstable, explicitly check its stability and if stable, add it to list of stable cones (i.e. protojets).

Algorithm applied to determinate splitting and merging of reconstructed stable protojets and to check minimal transverse momenta of these protojets, is as follows:

1. Remove all protojets with $p_T < p_{T,min}$.

2. Identify protojet i with highest p_T, i.e. highest sum of transverse momenta of particles creating given jet.

[1] $R = \sqrt{(\eta_j - \eta_i)^2 + (\phi_j - \phi_i)^2}$

3. Identify protojet j with highest p_T that shares particles with protojet i.
4. If such protojet exists, determine $p_{T,shared}$, i.e. sum of transverse momenta of particles belonging to both protojets i and j
5. If $p_{T,shared} < f p_{T,j}$, then assign particles in shared area to protojet, whose axis is closest. Otherwise, merge both protojets, adding it to list of protojets and removing original two.
6. If previous process created protojet that coincides with already existing one, keep new protojet as distinct form existing copies.
7. If non of the existing protojets shares particles with protojet i, add this protojet to list of final jets, removing it from protojet list.
8. Repeat this process until no protojet is in list of protojets.

1.2.2 Clustering algorithms

Clustering algorithms are based on sequential pair recombination of particles. It is simple and infra-red safe.

Most used is k_T jet-finder, based on [20], which copies backward QCD branching sequencing, therefore it includes more particles radiated from original hard parton thus having better energy resolution. Other algorithms used are Cambridge/Aachen[2] jet algorithm and anti-k_T[3] algorithm.

For comparison, in table Tab. 1.1 are complexities of different algorithms.

k_T algorithm

The definition of *inclusive* k_T jet algorithm is as follows:

1. For each pair of particles i, j calculate k_T distance:

$$d_{ij} = \min(k_{ti}^2, k_{tj}^2)\frac{\Delta R_{ij}^2}{R^2}$$

[2] Cambridge/Aachen algorithm is similar to k_T algorithm except calculation of d_{ij} is treated from geometrical point of view, i.e. $d_{ij} = \Delta R_{ij}^2/R^2$ and $d_{iB} = 1$.

[3] Anti-k_T algorithm is defined exactly as k_T algorithm except instead of transverse momenta it takes inverse transverse momenta as a distance measure.

Algorithm	Type	complexity
k_T	Sequential recombination	$N \ln N$
Cambridge/Aachen	Sequential recombination	$N \ln N$
Anti-k_T	Sequential recombination	$N^{3/2}$
SISCone	Cone algorithm	$N^2 \ln N$

Table 1.1: Jet reconstruction algorithm complexity, where N is number of particles to be processed.

where $\Delta R_{ij}^2 = (y_i - y_j)^2 + (\phi_i - \phi_j)^2$ and k_{ti} , y_i and ϕ_i are transverse momentum, rapidity and azimuthal angle of particle i and R is a jet-radius parameter usually taken ~ 1.

2. For each particle calculate beam distance $d_{iB} = k_{ti}^2$

3. Find minimum d_{min} of all d_{ij} and d_{iB}. If d_{min} is d_{ij}, then merge particles i and j into single particle, summing their 4-momenta (true for recombination scheme being E-scheme). If it minimum is d_{iB} then set particle i to be final jet and remove it from the list of particles.

4. Repeat from step 1 until no particles are left.

Exclusive longitudinally invariant k_T jet algorithm is similar to inclusive one, but when d_{iB} is the smallest value, then particle is considered to become part of beam jet and clustering is stopped when all d_{ij} and d_{iB} are above d_{cut}.

This algorithm is graphically depicted in Fig. 1.3a-Fig. 1.3f, showing application of k_T-algorithm on 5 particles. In Fig. 1.3a is initial configuration of particles. In Fig. 1.3b, first particle is taken to be a final jet, because its p_T is smallest of all d-parameters calculated. In Fig. 1.3c, two top particles are merged, because of close distance d-parameter is smaller than transverse momenta of given particles due to geometric part of definition of d-particle, and their d-parameter is smaller than any other such parameter. Similarly, two bottom particles are merged in Fig. 1.3d, having one jet that does not come into iterative process, and two 'particles' to be processed. In Fig. 1.3e, 'particle' on top of the figure has smallest transverse momentum and this transverse momentum is smaller than d-parameter between remaining 'particles', due to large distance between them, making it second final jet. In

Fig. 1.3f, because of no other particle to be merged with, last ‘particle’ is processed as third jet.

To conclude, three jets were created from five original particles after 5 iterations.

1.2.3 Jet Area

Package containing FastJet algorithms came with methods of finding jet areas. This area measures possibility of jet being affected by uniformly distributed background created by soft particles. It may be used to visualise jets and is liable to analytical treatment. Example of reconstructed jet areas is in Fig. 1.4. It is fount that not all cones have area πR^2.

There are three different definitions of areas in fastjet package and these are:

- *Active areas* add uniform background of extremely soft particles, ghosts, to event and cluster them. Softness of ghost ensures that these ghosts do not affect original set of particles inside a jet. Area of a jet is proportional to number of ghost inside this jet.

- *Passive areas* are fount by random placement of ghost and repeating this procedure. Passive area is proportional to probability of ghost being included inside a jet.

- *Voronoi area* is calculated by adding Voronois areas of particles constituting jet. These are calculated by determining Voronoi diagram for every event. For k_T algorithm Voronoi area coincides with its passive area.

Event with simulated jets is shown in Fig. 1.4, where jet areas are calculated and drawn with different colours.

1.3 Beauty tagging

Method used in this analysis for beauty tagging is secondary vertex reconstruction. It utilises relatively long lifetime of beauty mesons and baryons, listed in table Tab. 1.2.

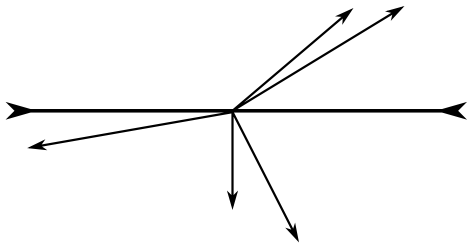

(a) initial configuration of particles detected in given event, before any iteration

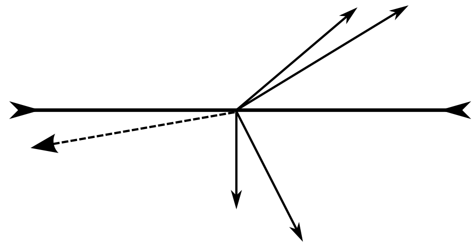

(b) first jet found, because of smallest d_{iB} between particle and incoming beam from set of all d_{ij}, d_{iB}

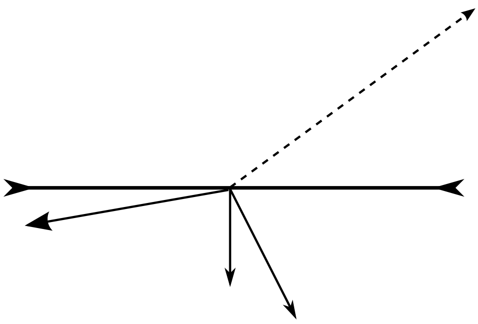

(c) upper two particles are merged due to having smallest d_{ij} from all d_{ij}, d_{iB}

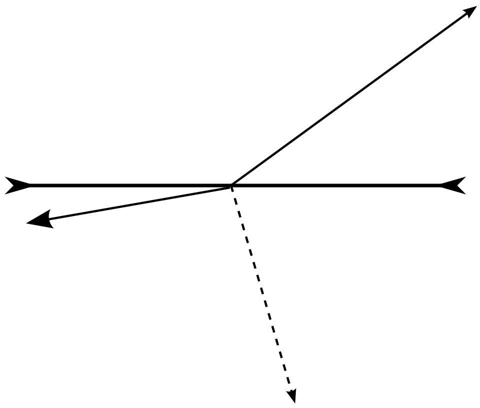

(d) lower two particles are merged for same reason as in case *c)*

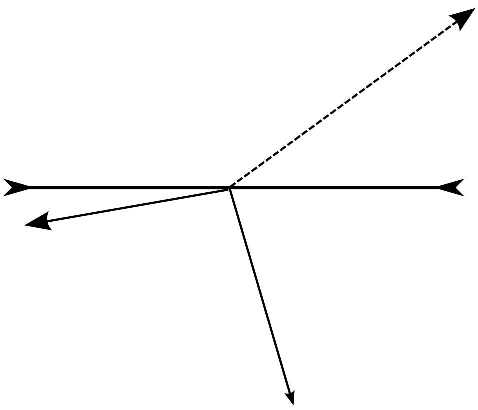

(e) smallest value is for d_{iB}, thus another jet is found

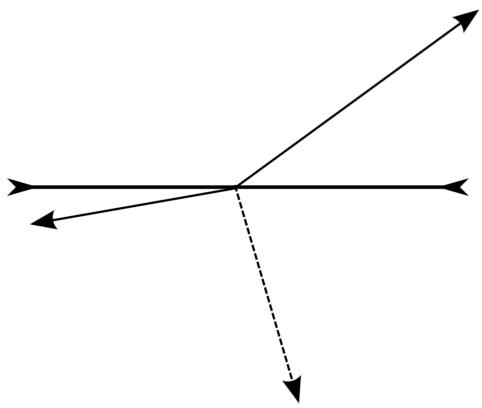

(f) final particle of the list has to be final jet

Figure 1.3: Schematics showing iterative process of finding jet using k_T algorithm, where small arrows signify particle's vector $\vec{k}$, large arrow already found jet and reversed arrows show incoming beams' paths. Dashed lines show $\vec{k}$ that underwent most recent iteration. Iteration proceeds alphabetically, from (a) to (f).

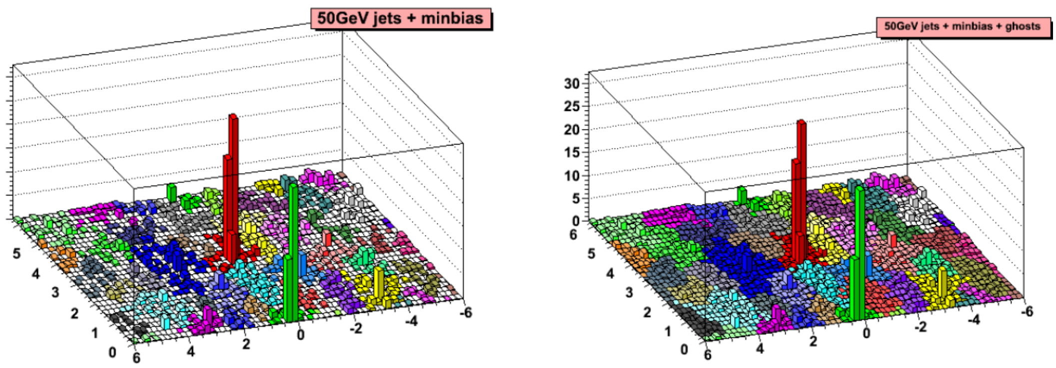

Figure 1.4: A simulated event at high luminosity at LHC. Left: A single event with two hard jets combined with 10 softer events. Right: Very soft 'ghost' particles added in order to quantify jet areas of each jet more precisely.

Particle	Quark content	Lifetime [ps]	$c\tau$ [mm]
B^+	$\bar{b}u$	1.638 ± 0.011	0.491 ± 0.003
B^0	$b\bar{d}$	1.530 ± 0.009	0.459 ± 0.003
B^0_s	$b\bar{s}$	1.417 ± 0.042	0.425 ± 0.013
B^+_c	$\bar{b}c$	0.463 ± 0.071	0.139 ± 0.021
Λ_b	udb	$1.383^{+0.049}_{-0.048}$	0.414 ± 0.014
Ξ_b mixture	$usb + dsb$	$1.42^{+0.28}_{-0.24}$	$0.425^{+0.084}_{-0.072}$

Table 1.2: Table of lifetimes of different hadrons containing beauty quark.

This method sequentially combines track pairs, looking for tracks close enough to previously reconstructed vertex or other tracks, then trying to add another track in such a way that it does not violate statistical fit.

Afterwards, looking to different properties of this reconstructed vertex, rejecting insufficient vertex candidates, for example with wrong direction of reconstructed momenta, insufficient mass, etc.

Another step in this analysis is rejection of V^0 candidates, this includes K^0_s, Λ and gamma conversions. These V^0 are created from track with opposite charges, in case of K^0_s these tracks are charged pions with invariant mass around 490 MeV. Λ has proton as one of decay products and invariant mass around 1100 MeV. For gamma conversions, invariant mass may vary significantly, but these usually reflect material occurrence. They are created with pairs of electron - positron with negligibly small opening angles in between them.

For example in measurement of b-quark jet shapes for CDF, [16], secondary vertex algorithm choose tracks with hits in at least 3 SVT layers, $\chi^2/d.o.f.$ equal to 8, i.e. sum of squares of the deviations between location of silicon hits and fitted tracks. Number of degrees of freedom is number of parameters used when fitting tracks to silicon hits. Track's $p_T > 0.5$ GeV/c and removal of conversions , K_s^0 and Λ has to be done. Impact parameters in transverse plane and in z-direction are smaller than 0.15 cm and 2.0 cm, respectively. These are to reduce interaction with material. Seed vertices have to have $\chi^2 < 50$.

1.4 Other methods

Other method, used to search for beauty or rather heavy flavour in general, is mainly probability jet algorithms.

This method looks into impact parameter significance of track, comparing it with resolution function of track coming from primary vertex and calculating its probability that it originates from primary vertex. In next step, probability for jet to originate in primary vertex is calculated from combined track probabilities.

Complementary to this algorithm is reconstruction of secondary vertex with V^0 rejection and usually serves as check of this algorithm.

More complex algorithms are likelihood algorithms that use predefined distributions from Monte-Carlo simulations. These simulations are used to compared with real data, giving likelihood for given discriminating variable. For tagging purposes, combined information from likelihood of different discriminating variables is used. As discriminating variables, invariant masses of reconstructed secondary vertices may be used as well as probabilities of jet originating in secondary vertex, and others.

Chapter 2

ALICE experiment

The Large Hadron Collider, LHC, is world's largest particle accelerating experiment, built to study collisions of protons with energies of 7 TeV and lead ions with energy of 1150 TeV. It is located in CERN, Centre for Nuclear Research in Geneva, Switzerland, at the border with France. LHC lies in a tunnel 27 km long, 100 meters under ground, and its magnets operate at 1.9 K, producing high magnetic field. Collider is composed of several main experiments, namely ATLAS, ALICE, CMS, LHCb, LHCf, TOTEM.

ALICE (A Large Ion Collider Experiment) is multi-purpose heavy-ion colliding experiment, one of LHC's main experiments, intended for study of strongly interacting matter and quark-gluon plasma. Additionally, it shall provide reference data from proton - proton and proton - nucleus collisions for heavy-ion collisions and address several QCD topics for which ALICE is complementary to other LHC's experiments. It's designed to deal with high particle multiplicities anticipated in lead - lead collisions.

ALICE, Fig. 2.1, consists of 18 different detection systems each specifically built. Central detection system inside solenoid magnet of up to 0.5T is composed of Inner Tracking System, ITS, Time Projection Chamber, TPC, Transition Radiation Detector, TRD, and Time-of-Flight detector,TOF. Complement to these central detectors in $|\ \eta\ | \leq\ 0.9$ and full azimuthal angle are cherenkov detectors in High-Momentum Particle Identification Detector, HMPID, further are ElectroMagnetic Calorimeter, EMCal, and Photon Spectrometer, PHOS. At large rapidities are placed Photon Multiplicity Detector, PMD, Forward Multiplicity Detector, FMD, and muon spectrometer. Additional systems include V0 and T0 system for faster triggering and Zero Degree Calorimeter, ZDC.[1]

2.1 Central detection systems

The innermost detector of ALICE experiment is Inner Tracking System. Its purpose is secondary vertex reconstruction, tracking and particle identification of particles with low momenta and improved measurements of impact parameters and track momenta. Detector is composed of 6 layers, 2 innermost are Silicon Pixel Detectors, SPD, next are 2 layers of Silicon Drift Detectors, or SDD, and outermost are Silicon micro-Strip Detectors, SSD.

SPD and SDD improve impact parameter resolutions, SDD and SSD are built in such a way that they can be used for particle identification via dE/dx measurement in non-relativistic region, making ITS low-p_T spectrometer, with relative resolution of 2% for pions in transverse momentum range from 100 MeV/c up to 3 GeV/c. Spacial resolution of ITS is of order of several tens of micrometres, with best resolution of $12\mu m$ for layers closest to primary vertex.

Following ITS, is Time Projection Chamber or TPC, main tracking detector, covering full azimuth and $\mid \eta \mid < 0.9$ for full track lengths, and $\mid \eta \mid < 1.5$ for reduced tracks. TPC covers wide range of transverse momenta, from 100 MeV/c up to 100 GeV/c, with good resolution. TPC's particle identification utilises particle energy loss in gass mixture of $Ne/CO_2/N_2$, reaching resolution of 5% for isolated tracks.

Covering TPC is Transition Radiation Detector, TRD, that utilises transition radiation of particles with higher momenta. Its purpose is electron-pion discrimination and position and momentum resolution enhancement.

For further particle identification, Time Of Flight detector, TOF, and High Momentum Particle IDentification, HMPID, are used. These enable better pion/kaon and kaon/proton differentiation. Later detector is optimised for identification of light nuclei and anti-nuclei, such as d, t, ^{3}He, α at high transverse momenta. TOF measures time of flight of particles using Multi-gap Resistive Plate Chamber and

[1]Data are from [6], [10] and [11].

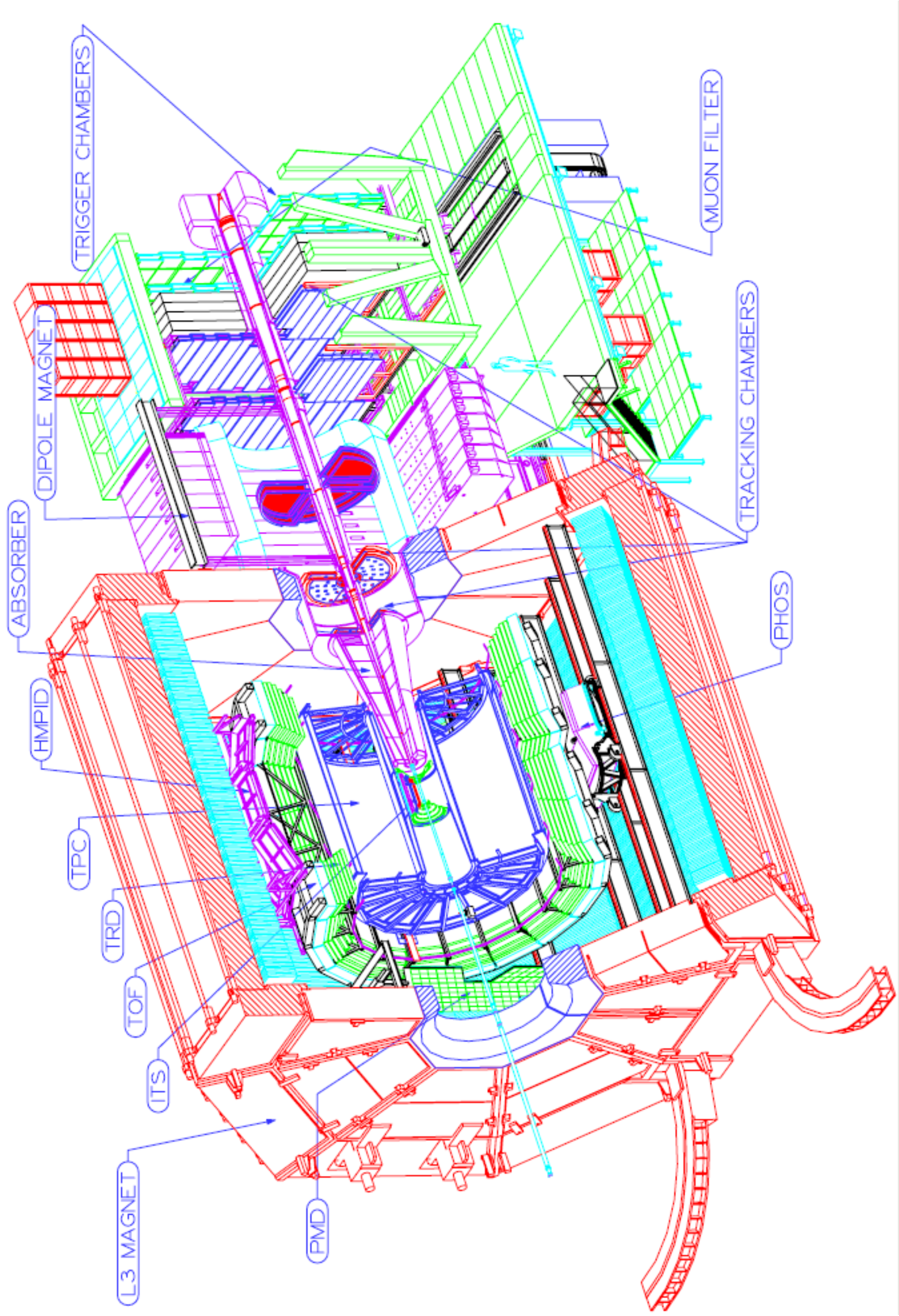

Figure 2.1: ALICE detectors

HMPID is based on focusing Ring Imaging Cherenkov counters.

With limited area domain in central rapidity lies PHOton Spectrometer, PHOS. Its purpose is direct photon measurement indicating initial phase of collision and study of jet quenching through high-p_T neutral pion and photon-jet measurement.

ElectroMagnetic Calorimeter is another detector enabling study of jet quenching in ALICE. It covers $|\eta| \leq 0.7$ and in azimuth it covers $\Delta\phi = 107°$. It is composed of Pb-scintillator sampling, located next to ALICE magnet at radius ~ 4.5 m with 12 672 towers having $\Delta\eta\times\Delta\phi \approx 0.0143\times0.0143$ at midrapidity. EMCal's resolution should be $10\%/\sqrt{E}$

2.2 Tracking and identification

For tagging of beauty hadron, particle identification and tracking are necessary for precise secondary vertex position estimation or precise measurement of impact parameter, depending on method chosen for tagging.

2.2.1 Tracking

Track reconstruction in central region is done via ITS, TPC and TRD. Tracking itself, begins in TPC, best tracker present, where overall efficiency of track reconstruction is 85% for all transverse momenta and resolution of track's energy loss is around 6%, [6]. Firstly, track candidates, seeds, are found and tracking proceeds to smaller radii of TPC, where new clusters are associated to existing seeds if possible, thus refining track parameters.

Second step is prolongation of tracks to ITS, when all seeds are prolongated to inner radii of TPC. Here, tracks are prolongated to primary vertex and precise ITS clusters are associated to track candidates. Also, in ITS impact parameters are calculated with respect to previously found primary vertex. To some degree, data from TRD help in improvement of momentum resolution of tracks.

In the last step, cascades, V^0's and kinks from secondary vertices are reconstructed using reconstruction algorithm in ITS and TPC. V^0 reconstruction, i.e. reconstruction of neutral particles from pair of tracks with opposite charge as depicted in Fig. 2.2, is done by selecting secondary tracks with sufficient impact parameters.

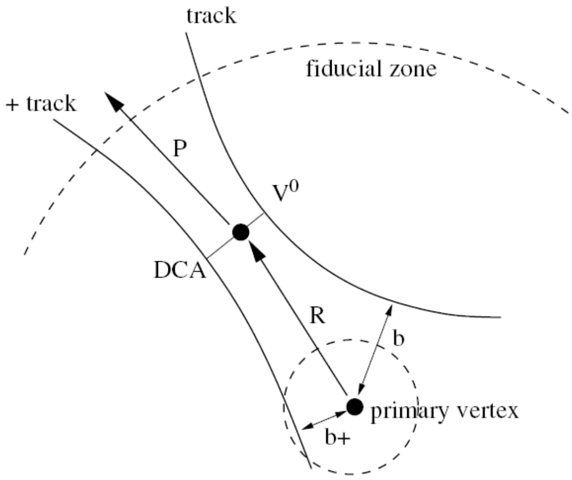

Figure 2.2: V0 reconstructed using tracks of opposite charges, with sufficient impact parameters, b, and small enough distance of closest approach

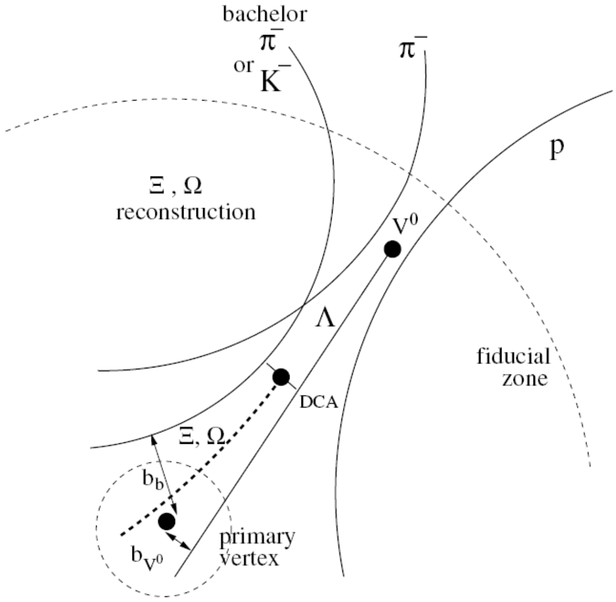

Figure 2.3: Reconstruction of cascade decay of Ω^- (Ξ^-) through Λ^0

Afterwards, combinations of 2 tracks of opposite charge create possible secondary vertices. These are rejected based on DCA cut placed on these two particles, and position of this closest approach. As last, momenta of V^0 is checked with respect to primary vertex.

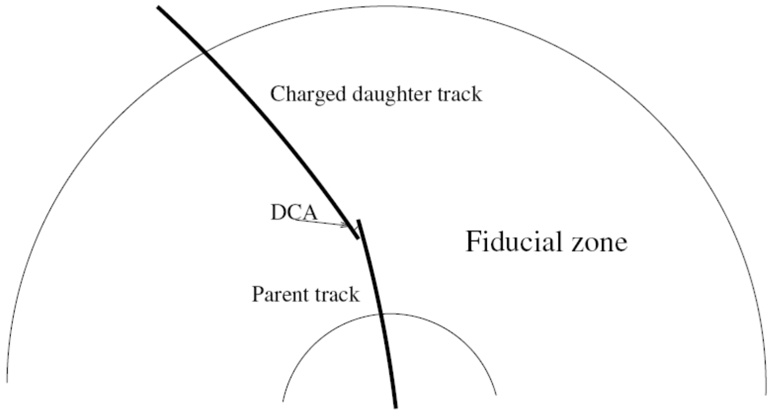

Figure 2.4: Kink, signature of 1-prong decay

Similarly, cascade, subsequent decays of decay particle created, reconstruction starts with search for V^0 with large impact parameter, Fig. 2.3 depicts cascade decay of Ω^- (Ξ^-) through Λ^0 as V^0. Next is selection of secondary track candidate, with small enough DCA to calculated trajectory of V^0. Again, momentum at this decay vertex is check with respect to primary vertex.

Reconstruction of kinks, Fig. 2.4, sign of 1-prong decay like $K \rightarrow \mu\nu$ or $\pi \rightarrow \mu\nu$, is done by finding 2 tracks of same charge with small DCA.

2.2.2 Particle identification

Information for particle identification (PID) of charged particles is provided by ITS, TPC, TRD, TOF and HMPID detectors.

ITS provides information in non-relativistic region . In cases of low momentum particles, it is the only source of their type. In this detector, energy is deposited to silicon detectors.

In TPC, charged particles ionize gas and lose energy. This lost energy is measured and compared to prediction from Bethe-Bloch's formula, probability distribution is calculated for all particle types based on calculations.

TRD detector mainly differentiates between electrons and pions. As name signifies, it uses transition radiation for identification. Similarly, TOF detector utilizes time signatures matching reconstructed tracks and HMPID is detector designed to help identify hadrons with high momenta. With it's help, for electron identification efficiency of 90%, pion suppression of two orders is achieved.

Combining information from different detectors is complicated but necessary, because identification in certain region and detector may have different weight than in other detector. For example, signal for the different particle types at given momenta may be same for one detector, but completely different in second detector.

2.2.3 ALICE performance

First proton beams circulated in LHC on 10th September 2008, but on 19th September, accident involving quenching of magnets occurred, delaying first collisions for more than a year. These happened on 23rd November 2009 at $\sqrt{s}$ = 900 GeV. Few days later, 28th November, first paper, [4], was submitted, with 284 recorded events.

In Fig. 2.5a, published in [4], z-coordinate of reconstructed collision vertex by ITS from these events is seen, and in Fig. 2.5b, from same source, multiplicities of charged particles for inelastic and non-single diffractive collisions with respect to pseudo-rapidity are plotted, compared to data from proton-antiproton collisions from UA5 experiment.

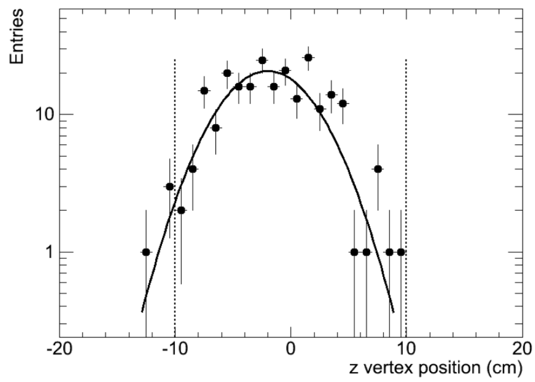

(a) Longitudinal vertex distribution from hit correlation in two pixel layers of ITS.

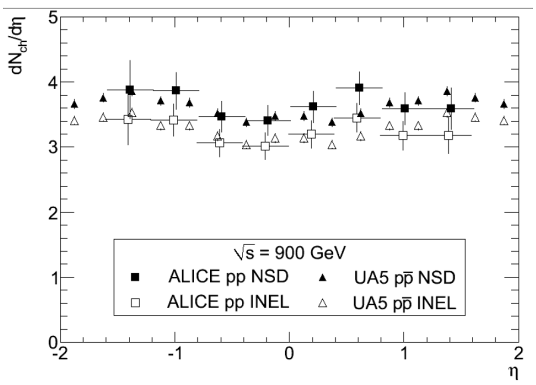

(b) Pseudo-rapidity dependence of number of charged particles for INEL and NSD collisions. ALICE measurements are squares, UA5 are triangles.

Figure 2.5: Results obtained from first data in ALICE, longitudinal vertex distribution, (a), and pseudo-rapidity dependence of charged particles multiplicities, (b). Plots are taken from [4].

On 30th March 2010, highest energy of protons accelerated by human was reached, producing collisions at centre of mass energy $\sqrt{s} = 7$ TeV. These proton-proton collisions should take place for another year with pause for heavy-ion collisions in autumn. Afterwards, long shutdown is planned for LHC upgrade to reach the designed maximum energy.

From results published in [2], [3] and [4], we see that ALICE detectors and reconstruction algorithms have very good performance.

Chapter 3

Data Analysis

In this chapter, analysis of simulated data is presented. The aim was to measure properties of b-tagged jets.

For this analysis, I used official software produced by and for ALICE group in CERN. In this work I used `AliRoot` version `v4-18-Rev-06`. Compatible version of `Root` used was `v5-26-00b`, version `v8-125` of `Pythia8` and `v3-1-11` and `v4-9-2-p02` of `GEANT3` and `GEANT4`, respectively.

Furthermore, for jet analysis were `FastJet` and `SISCone` packages used. Their versions are `v2-4-1` and `v2-0-1`, respectively.

3.1 Data used

In this analysis, data downloaded from *GRID* was used, located in /alice/sim/PDC_08b/LHC08d10. I used files located in directories 50 000 to 50 027, having 27 224 *AliESDs.root*[1] files in total. Each such file contains 200 events, thus producing 5 324 800 events in analysis, not counting corrupted files.

3.1.1 MC data

For production of these data, `Root` version is `v5-23-04`, `GEANT3` version is `v1-10-1` and `AliRoot` version is `v4-16-Rev-12`. Data were produced 1.-2.6.2009 and con-

[1]ESD meaning Event Summary Data.

tain proton-proton collisions at centre of mass energy of 14 TeV, producing at least one beauty quark-antiquark pair per event.

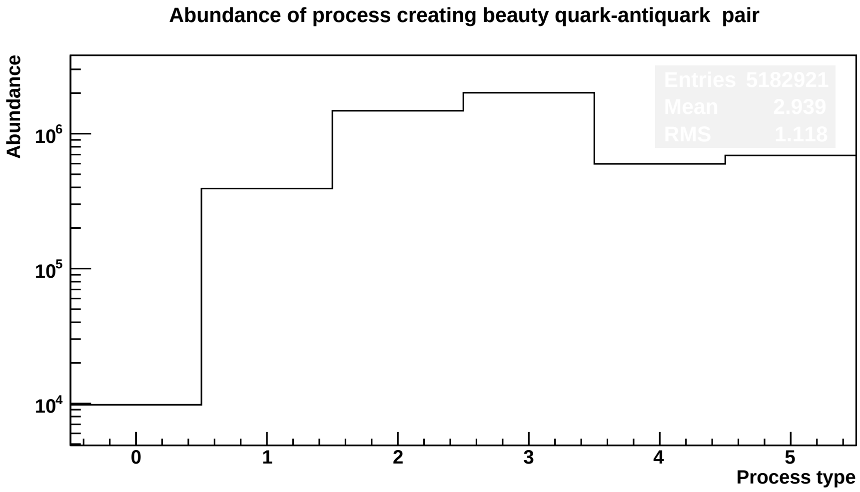

Figure 3.1: Types of processes in simulated data samples from which beauty quarks originate are (0.) quark pair creation, (1.) pair creation from gluon, 2. flavour excitation, (3.) gluon splitting. (4.) initial-state parton shower and (5.) light parton shower.

As seen in Fig. 3.1, origin of beauty quarks in simulation is taken into consideration, varying from pair creation, flavour excitation to gluon splitting, this being most common process creating heavy quarks.

When selecting events in real data, position along beam is taken into consideration in order to prevent bias, that would be created, if collision did not happen in the center of central detectors. For this purpose, component parallel to beam of position vector of primary vertex from origin taken at the centre of central detector system shall not exceed predefined value. This displacement of vertex from origin in z-direction is in this analysis smaller than 20 cm.

In sample used in my analysis, such event selection was unnecessary, because as seen in Fig. 3.2, Z-coordinates of primary vertices generated, Fig. 3.2a, and reconstructed, Fig. 3.2b, are nearly identical. The difference between reconstruction and simulation of primary vertex are small, as seen in Fig. 3.2c.

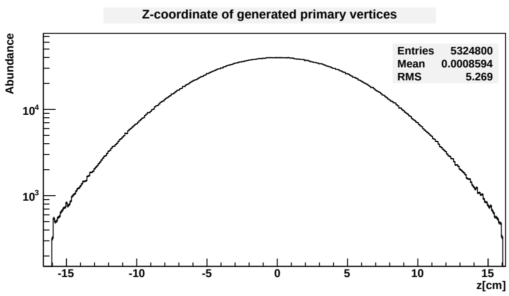

(a) Generated position of primary vertex.

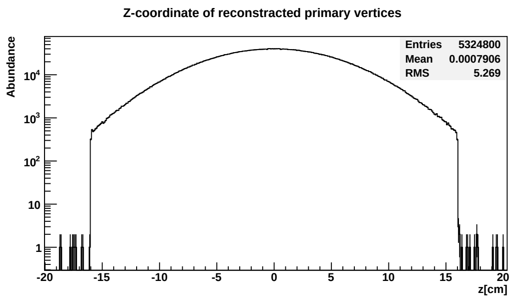

(b) Reconstructed position of primary vertex.

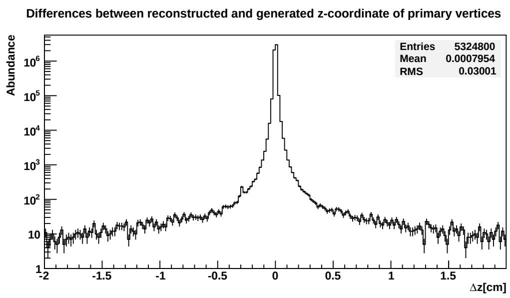

(c) Difference in reconstructed and generated position of primary vertex.

Figure 3.2: Position of primary vertex of collision as generated, (a), as reconstructed, (b), and difference between reconstructed and generated position, (c).

Beauty quarks

Concerning beauty quarks, in every event at least one pair of beauty flavoured quark-antiquark pair is created, as seen in Fig. 3.3. As expected, predominantly, only one such pair is created. This case is 97.34% of all events. Limit of four beauty quark anti-quark pairs created in 15 out of 5 324 800 collisions is reached.

Spectra of transverse momenta of produced beauty quarks and anti-quarks are plotted in Fig. 3.4. Both spectra, for quarks and anti-quarks, are nearly identical, as expected, with most common $p_T^{mode} \approx 4$ GeV/c and mean value at $p_T^{mean} = 23.21$ GeV/c.

These quarks and anti-quarks are distributed into pseudo-rapidity region $\eta \in \langle -7, 7 \rangle$, as seen in Fig. 3.5. More than 75% of beauty quarks and anti-quarks was

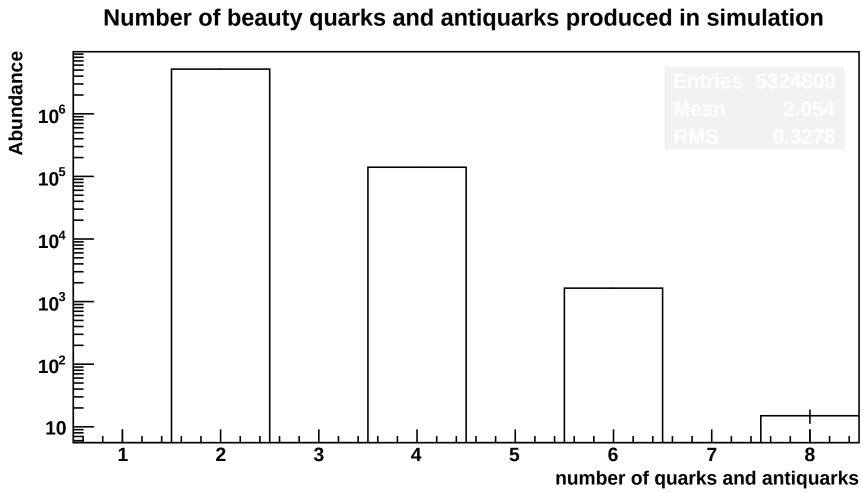

Figure 3.3: Number of produced beauty quarks and anti-quarks in event.

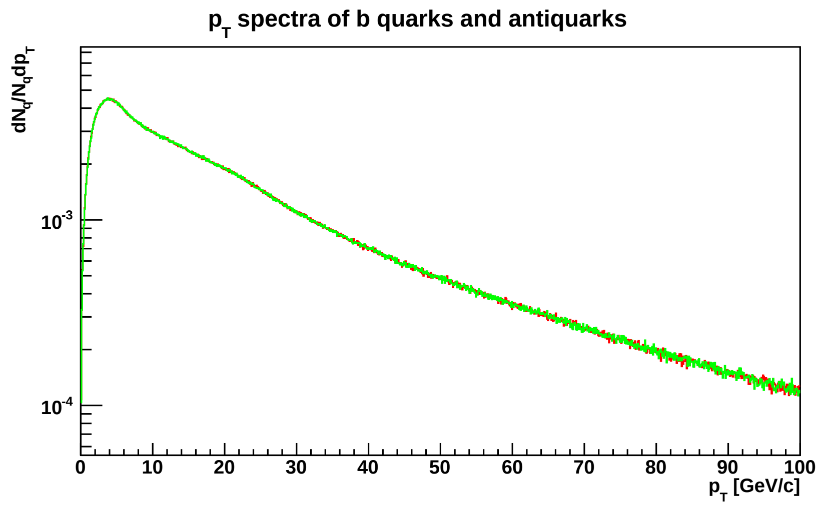

Figure 3.4: Spectra of transverse momenta of produced beauty quarks (green line) and anti-quarks (red line).

produced into region of $\eta \in \langle -2, 2 \rangle$, with maximum at mid-rapidity.

Hadrons containing beauty quark

From beauty quarks all kinds of different hadrons may be created. These are summarised in table Tab. 3.1, with their abundances and relative occurrences in ana-

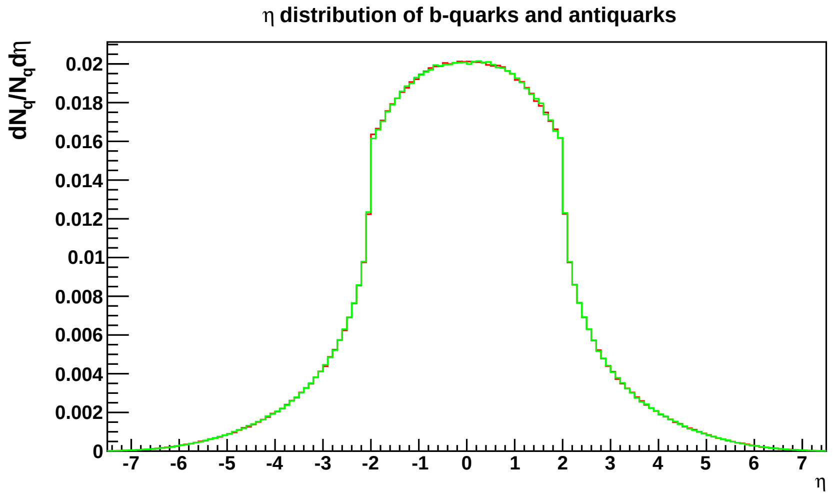

Figure 3.5: Pseudo-rapidity distribution of quarks (green line) and antiquarks (red line).

lysis. Undergoing processes like de-excitation or decay into more stable hadron with beauty flavour, reduces these hadrons into several final hadrons, summarised in table Tab. 3.2. Dominant particles are B-mesons with long enough lifetimes, as mentioned previously in Tab. 1.2.

These final hadrons have decay vertex displaced from primary one. This displacement in transverse xy-plane is shown in Fig. 3.6.

Some decay lengths longer than expected may be explained by multiple radiations and decays before these final beauty hadrons are created. These processes may be more multifarious than in real collisions, because I expect some enhancement due to layout of simulation, being production of beauty jets[2].

Beauty hadron may undergo processes like radiation or decay into other beauty hadron. In such a process cosine of angle between original and daughter hadron is shown in Fig. 3.7a. It is observed dominant production into small angles from original hadron's direction and relatively increased production into small angles around π radians from direction of original hadron. Also, relative energy loss by radiation or decay is in general small, but fraction of energy carried by daughter particles and energy of original hadron may in some cases exceed 1, as seen in

[2] Production details, like simulation `Config.C` file, were not available on GRID. No `jdl` file was available.

Name	Abundance	Rel. occurrence	Name	Abundance	Rel. occurrence
B^{*+}	1 536 578	14.43%	B^{*-}	1 623 938	15.27 %
B^{*0}	1 530 894	14.38%	$\bar{B}^{*0}$	1 629 446	15.30%
B_c^{*+}	862	0.01%	B_c^{*-}	6 870	0.06%
B_s^{*0}	456 780	4.29%	$\bar{B}_s^{*0}$	491 104	4.61%
B^+	511 590	4.80%	B^-	543 030	5.10%
B^0	512 444	4.81%	$\bar{B}^0$	533 600	5.01%
B_c^+	4 496	0.04%	B_c^-	33 442	0.31%
B_s^0	156 922	1.47%	$\bar{B}_s^0$	175 092	1.64%
Λ_b^0	209 160	1.96%	$\bar{\Lambda}_b^0$	158 912	1.49%
Ω_b^{*+}	434	0.00%	Ω_b^{*-}	6 596	0.06%
Ω_b^+	18 978	0.18%	Ω_b^-	53 330	0.50%
Σ_b^{*+}	82 336	0.77%	Σ_b^{*-}	64 634	0.61%
Σ_b^{*0}	46 434	0.44%	$\bar{\Sigma}_b^{*0}$	43 780	0.41%
Σ_b^+	41 974	0.39%	Σ_b^-	30 766	0.29%
Σ_b^0	18 800	0.18%	$\bar{\Sigma}_b^0$	9 366	0.09%
$\Xi_b'^+$	2 204	0.02%	$\Xi_b'^-$	2 414	0.02%
$\Xi_b'^0$	2 856	0.03%	$\bar{\Xi}_b'^0$	3 682	0.03%
Ξ_b^{*+}	5 228	0.05%	Ξ_b^{*-}	6 916	0.06%
Ξ_b^{*0}	10 212	0.10%	$\bar{\Xi}_b^{*0}$	17 938	0.17%
Ξ_b^+	21 654	0.20%	Ξ_b^-	20 074	0.19%
Ξ_b^0	15 058	0.14%	$\bar{\Xi}_b^0$	5 052	0.05%
Υ	1 716	0.02%			

Table 3.1: Table of hadrons produced from beauty quarks or anti-quarks.

Fig. 3.7b, where this is true for value on x-axis smaller than 0.

Decays of last hadron in cascade of decays and radiations of beauty hadrons generally produce up to several daughter particles, their number is in Fig. 3.8. Beauty hadrons are decaying up to 11 products, representing 0.008% of all decays. Such decays are for example decays 3.1,3.2 and 3.3. Mean number of daughter particles is 3.45 and 3 daughter particles occur in 19.679% of all cases.

$$B^0 \to \pi^- + \pi^+ + \omega + \pi^- + \pi^+ + \omega + \pi^- + \pi^+ + \pi^- + \pi^0 + \pi^+ \tag{3.1}$$

$$B^+ \to \rho^0 + K^{*+} + K^{*-} + \pi^+ + \pi^0 + \pi^- + \eta' + \pi^+ + \pi^0 + \pi^- + \pi^+ \tag{3.2}$$

Name	Abundance	Rel. occurrence	Name	Abundance	Rel. occurrence
B^+	2 126 128	19.96%	B^-	2 092 182	19.65%
B^0	2 120 026	19.91%	$\bar{B}^0$	2 091 652	19.64%
B_c^+	668	0.01%	B_c^-	9 348	0.09%
B_s^0	633 390	5.95%	$\bar{B}_s^0$	627 960	5.90%
Λ_b^0	422 668	3.97%	$\bar{\Lambda}_b^0$	4084 04	3.83%
Ω_b^+	566	0.01%	Ω_b^-	942	0.01%
Λ_b^+	29 036	0.27%	Λ_b^-	29 796	0.28%
Λ_b^0	28 490	0.27%	$\bar{\Lambda}_b^0$	15 696	0.15%
Υ	12 626	0.12%			

Table 3.2: Table of final beauty hadrons in cascade of hadrons containing beauty quark.

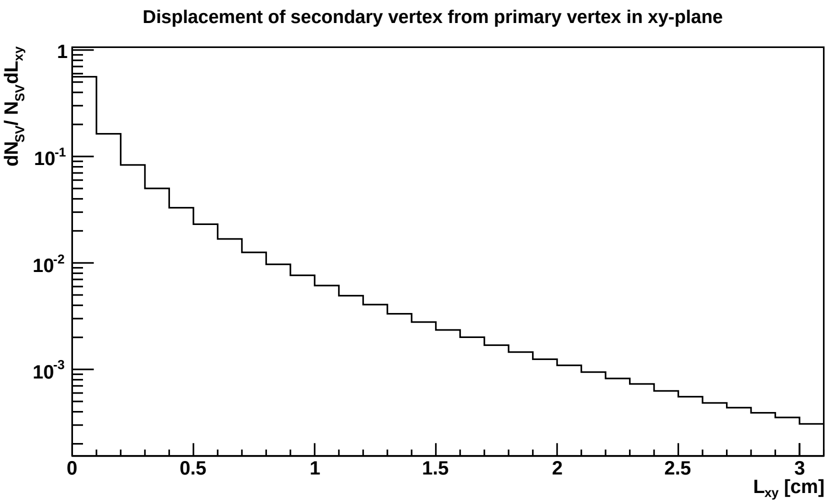

Figure 3.6: Displacement of secondary vertex, decay position of last beauty hadron, from primary vertex in transverse, xy-plane.

$$\bar{B}^0 \to D^+ + \pi^- + \pi^+ + \pi^- + \pi^+ + \pi^0 + \rho^0 + \pi^0 + K^{*-} + K^+ + \pi^- \tag{3.3}$$

Directly, 774 876 electrons or positrons was produced, giving in average more than one electron or positron per five events. Other decay products of these beauty hadrons are summed up in table Tab. 3.3. Fact that most common daughter particles

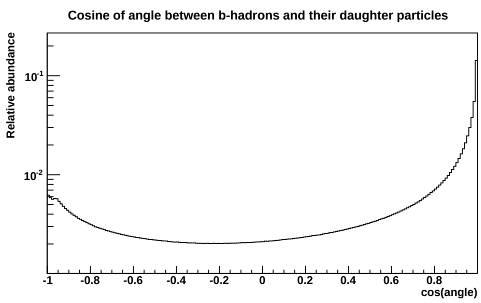

(a) Cosine of angle between original beauty hadrons and daughter particles.

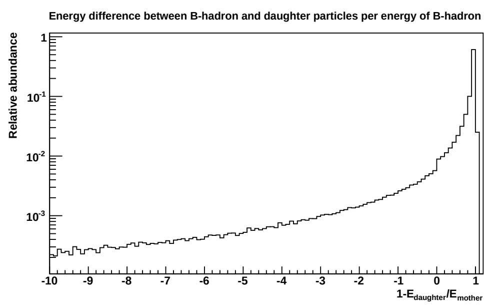

(b) Fraction of energy difference between beauty hadron's energy and its daughter products per energy of original hadron.

Figure 3.7: Properties of daughter particles of beauty hadron decays when decaying to other beauty hadron.

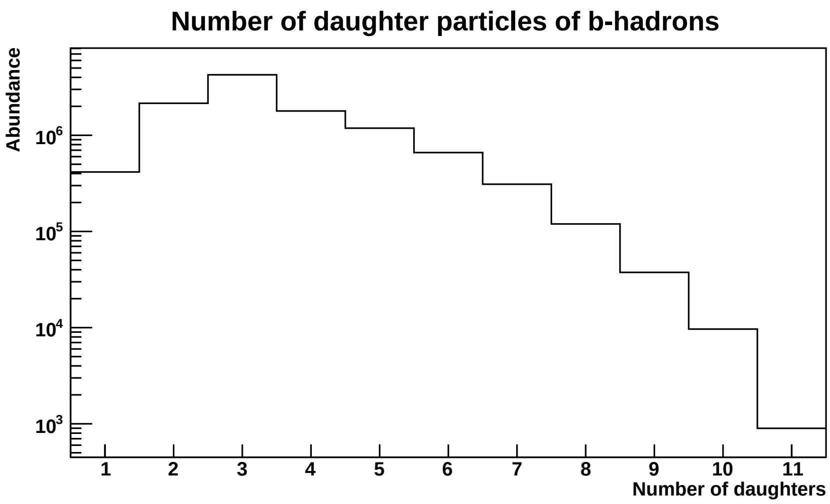

Figure 3.8: Plot showing number of decay products of last hadron containing beauty quark, i.e. last hadron of cascade of hadrons radiating and decaying whilst still creating hadron containing beauty quark.

from such a decay are pions, kaons, photons and D-mesons is not surprising.

Track reconstruction

Concerning tracks reconstructed in simulation, their number per event is shown in Fig. 3.9a, with maximum of approximately 300 tracks. On average, 67 tracks

Particle family	Abundance	Particle family	Abundance
D-mesons	11 354 325	Δ	79 723
J/Ψ	111 219	K-mesons	3 055 550
Λ	788 839	Ω	1 210
Σ	32 302	Ξ	156 001
A1 resonance	180 196	χ	182 509
η	1 326 973	g	293 720
l+ν_l	2 800 664	ω, ϕ, ρ	6 599 791
π	5 781 636	Nucleons	2 246 761

Table 3.3: Decay products of last hadron containing beauty quark.

were created, with most frequent number being 56. Most commonly, were tracks identified as pions, with more than 30% of all tracks. Kaons make for more than 20%, similarly, muons make nearly same amount. p_T spectrum of reconstructed tracks is in Fig. 3.9b.

For this track reconstruction, general particle identification was used, utilising probability distributions for given track to be given particle type, i.e. either electron, muon, pion, kaon or proton. For analysis, tracks having TPC and ITS refits and combined detector particle identification probability distributions[3] have been selected.

Reconstructed electrons

Data sample used contained 571 206 reconstructed electrons originating from decay of beauty flavoured hadron, 523 566 electrons from hadrons containing charm quark and 7 825 216 electrons that do not originate in heavy flavoured hadron.

Spectra of produced electrons can be fount in Fig. 3.10a. These spectra are normalised to the number of electrons of given origin, that is the reason behind beauty flavoured electrons dominating from approximately 4 GeV/c. This implies that probability of production of electron with transverse momentum greater than this value from beauty quark is higher than probabilities of producing same electron from other source.

Taking into account number of produced electrons per p_T bin, Fig. 3.10b, elec-

[3] In analysis, these are ensured by `kTPCrefit`, `kITSrefit` and `kESDpid` in track status.

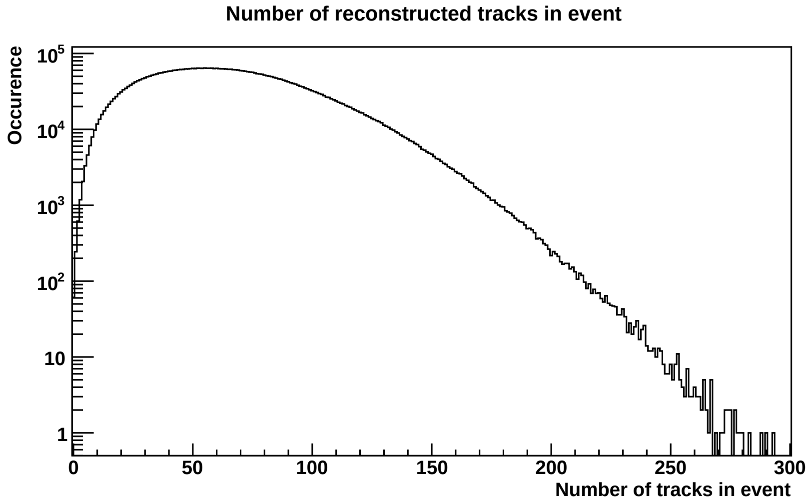

(a) Number of reconstucted tracks per event.

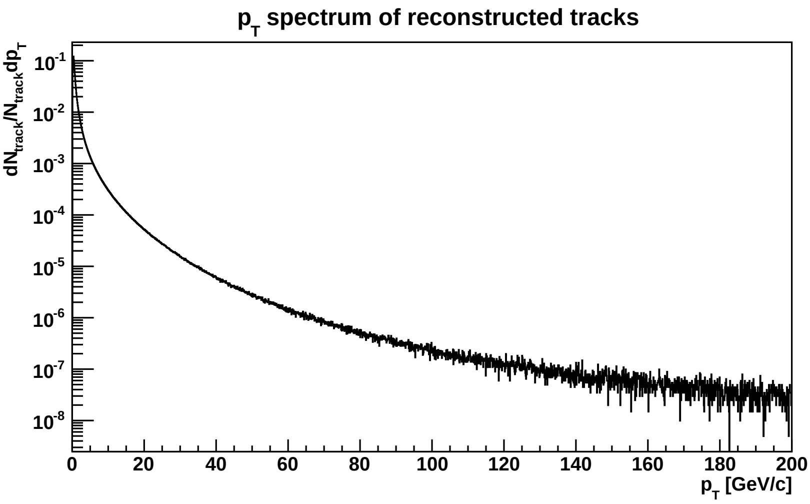

(b) p_T spectrum of reconstructed tracks.

Figure 3.9: (a) Number of reconstructed tracks per event. (b) p_T spectrum of reconstructed tracks.

trons from heavy flavour in this analysis become dominant constituent of all electrons at transverse momenta greater than 60 GeV/c.

In Fig. 3.11, relative transverse momenta difference in reconstruction with respect to generated transverse momenta generated are plotted for different p_T bins of generated tracks.

Distributions of impact parameters, i.e. signed distances of closest approach to

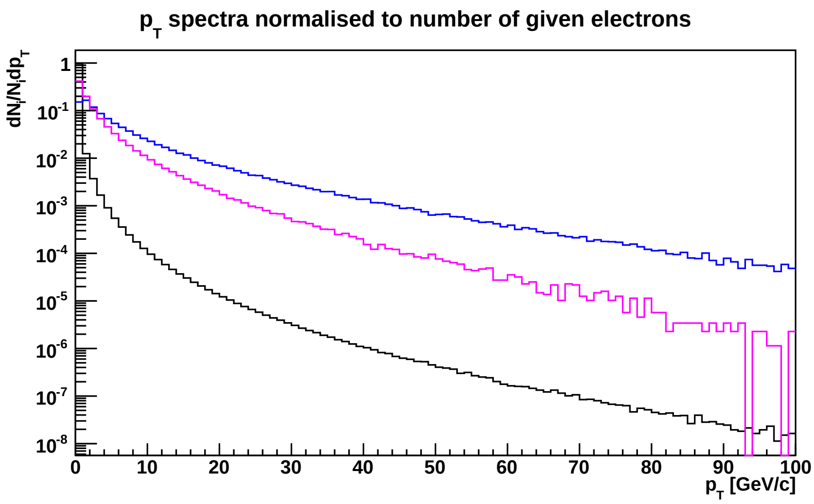

(a) p_T spectra of reconstructed electrons normalised by number of electrons from given origin.

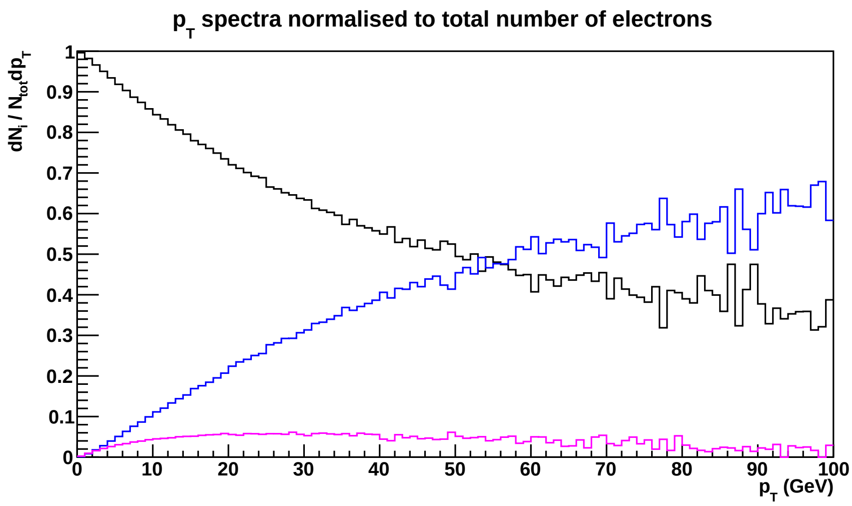

(b) p_T spectra of reconstructed electrons normalised per bin.

Figure 3.10: p_T spectra of reconstructed electrons with respect to flavour of their mother particle, blue are electrons from b-hadrons, magenta line represent c-hadrons and black line all the other electrons. Histogram line in 3.10a are normalised to the number of electrons coming from given source, in case of 3.10b, bins are normalised to the total number of electrons in given bin.

primary vertex, in transverse plane is plotted in Fig. 3.12. These distributions are normalised to total number of electrons of given origin. Electrons from sources

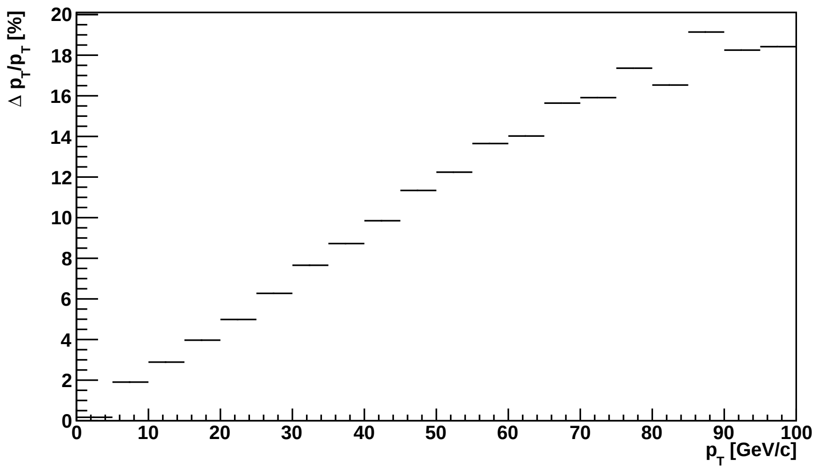

Figure 3.11: Relative transverse momenta loss for electrons with respect to transverse momenta of generated tracks.

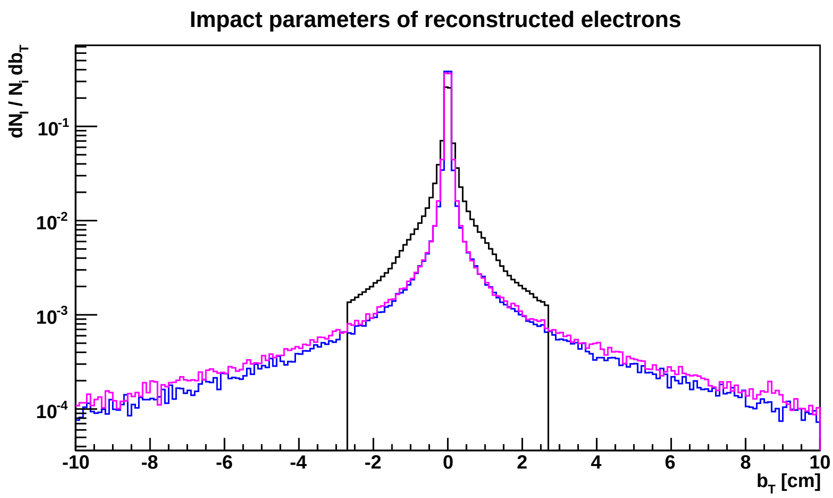

Figure 3.12: Impact parameter distribution normalised to number of electrons from given source, these are b-hadrons (blue line), c-hadrons (magenta line) and all the other electrons (black line).

other than heavy flavoured hadrons, dominate region of $|\ d_{xy}\ | < 3$ cm. Outside this region they are not present in data sample used for this analysis and electrons from b-hadrons and c-hadrons are equally distributed here.

3.2 Jet reconstruction

As mentioned at the beginning of this chapter, for jet analysis `FastJet 2.4.1`[4] and `SISCone 2.0.1`[5] packages were used.

For purpose of this analysis, `FastJet` used $R = 1.0$ and best recombination strategy, i.e. algorithm selecting strategy most suitable for given number of particles. k_T algorithm was chosen with energy scheme as recombination scheme, standard scheme as recommended in [7]. From two options of jet outputs, inclusive jets were selected, with transverse momenta of at least 10 GeV/c.

`SISCone`, cone algorithm, used radius $R = 1.0$. Ratio f defining energy fraction necessary to merge two overlapping cones was set to $f = 0.5$ and again minimal transverse energy of protojets was set 10 GeV/c. From jet merging several problems may arise, such as, when two jets are merged, we are unable to determine effective cone radius, i.e. minimal radius of cone necessary to include particles creating two original jets as it is not constant in all directions in $\eta - \phi$ space. Also overestimation of cone radius, as would be done in case of taking radius as distance between jet direction and the most displaced particle in above mentioned space, would include particles that do not necessarily create any of originally merged jets.

3.2.1 Comparison of reconstucted jets by SISCone and FastJet

Analysing same data sample by both algorithms independently, we find number of reconstructed jets to differ. Maximal number of SISCone jets per event, as seen in Fig 3.13a, is 7 in 27 cases, standing for less than 0.0001% of all the events in analysis. On the other hand, FastJet reconstructed in 6 cases 9 jets. Number of reconstructed FastJet jets is plotted in Fig. 3.13b. At least one jet was reconstructed in 82.83% of events in FastJet, whereas cone algorithm reconstructed at least one jet in 86.22% of events.

Comparing energy distributions of jets reconstructed by SISCone, Fig 3.14a, and FastJet, Fig 3.14b, algorithms shows, that clustering algorithm leads to jets with higher energies, as seen from generally shallower slope in normalised energy distributions in case of FastJet and more rapid fall in case of SISCone.

[4] Obtained from [26].

[5] Obtained from [27].

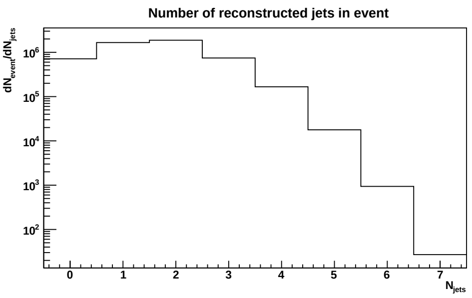

(a) Number of reconstructed jets per event with SISCone algorthm.

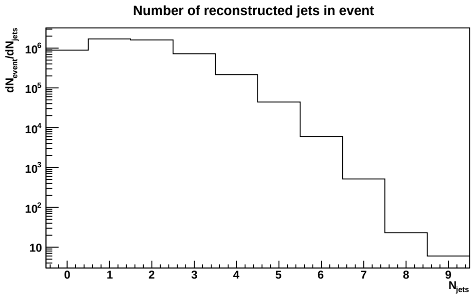

(b) Number of reconstructed jets per event with FastJet algorithm.

Figure 3.13: Number of jets reconstructed per event in case of SISCone, (a), and FastJet algorithm, (b).

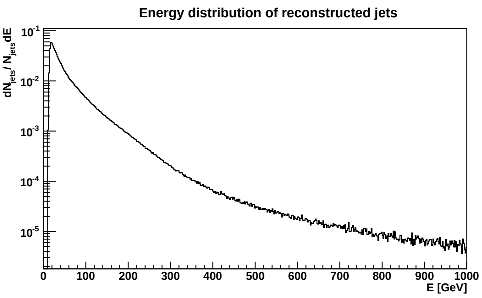

(a) Energy distribution of jets reconstructed with SISCone algorithm.

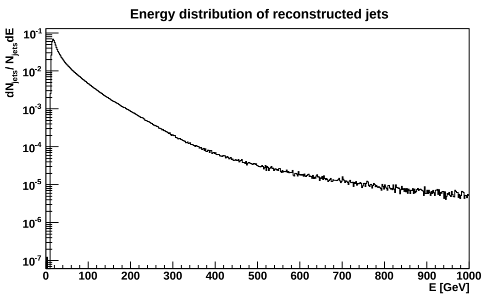

(b) Energy distribution of jets reconstructed with FastJet algorithm.

Figure 3.14: Energy distributions of jets reconstructed with SISCone algorithm, (a), and FastJet, (b).

Both SISCone and FastJet jets are reconstructed in region of pseudo-rapidity, $|\ \eta\ | < 1.6$, having only 3 cases in SISCone and 4 in FastJet outside of this region. These stand for particles with high 4-momenta, at the acceptance limit of inner ALICE detectors. Jets reconstructed with SISCone algorithm are reconstructed mainly around $\eta = 0$, Fig. 3.15a. However, FastJet jets have peaks in pseudo-rapidity distribution located at approximately ± 0.75, with slight depression in region of $\eta = 0$, as seen in Fig. 3.15b. Otherwise, they have generally same behaviour. This may be due to SISCone's merging of cones, producing from 2 or more jets not located in mid-rapidity region one jet in this region. This can be suppressed by smaller radius of cone and higher energy fraction necessary for merging procedure to take place.

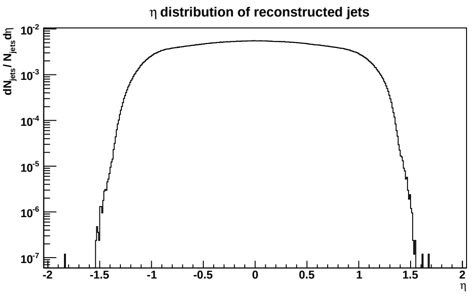

(a) Pseudo-rapidity distribution of jets reconstructed with SISCone algorithm.

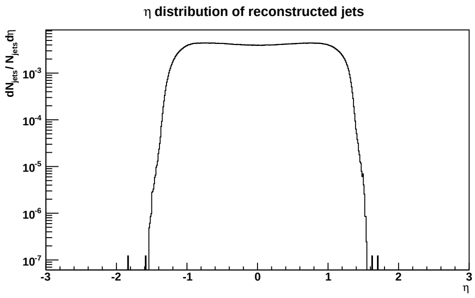

(b) Pseudo-rapidity distribution of jets reconstructed with FastJet algorithm.

Figure 3.15: Pseudo-rapidity distribution of jets reconstructed with SISCone and FastJet algorithms.

Concerning azimuthal distribution of reconstructed jets, these are fairly similar as seen from Fig. 3.16a and Fig. 3.16b, both showing a slight depression at $\phi = 0$. This depression is more significant in case of jets reconstructed with SISCone algorithm.

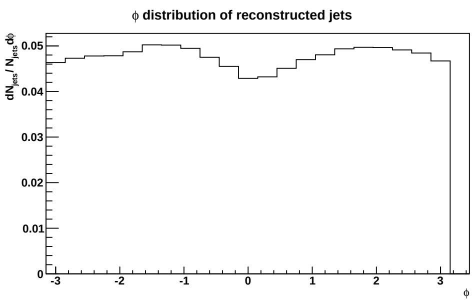

(a) Distribution of azimuthal angle of reconstructed jets using SISCone algorithm.

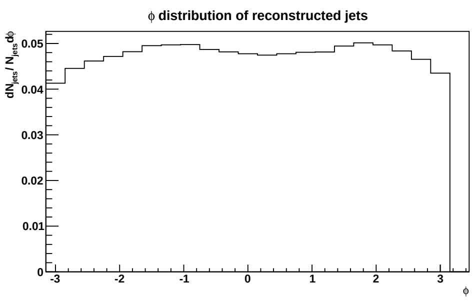

(b) Distribution of azimuthal angle of reconstructed jets using FastJet algorithm.

Figure 3.16: Distribution of azimuthal angles of jets reconstructed using SISCone, (a), and FastJet algorithm, (b).

In events with multiple jets, these jets are in $\eta - \phi$ phase-space displaced from each other mainly around value of $\Delta R \approx 3.14$, as seen in Fig. 3.17c and Fig. 3.17d. Maximal distances between jets in $\eta - \phi$ phase-space are in case of FastJet 4.1 with minimal one being 0.5. On the other hand due to possibility of overlap of two jets, SISCone's smallest distance between two jets is 0.1 and may reach 4.2.

Maximum at value of approximately 3.14 in ΔR -distribution represents back-to-back jets with angle between their momenta vectors approximately π radians, as seen in Fig. 3.17a and Fig. 3.17b, where peak is observed at value of cosine of angle between jets equal to -1. Slight increase is observed at angles approximately right angles, that may represent events with 4 beauty quarks produced.

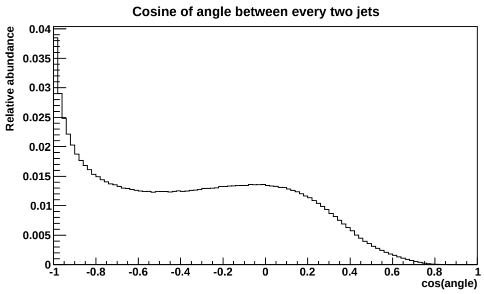

(a) Cosine of angle between every two jets in analysis done using SISCone algorithm.

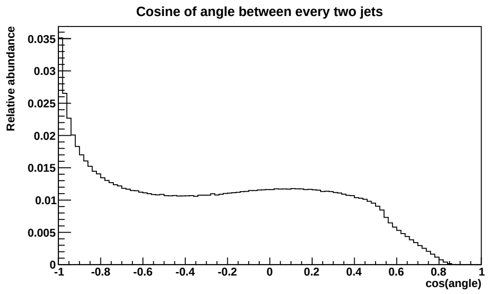

(b) Cosine of angle between every two jets in analysis done using FastJet algorithm.

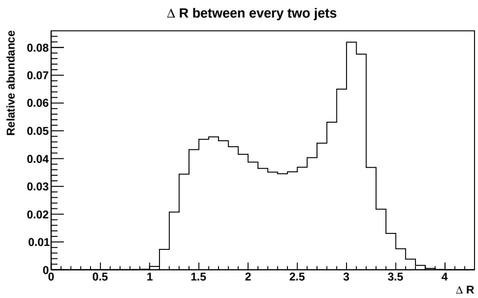

(c) Distance in $\eta - \phi$ space between every two jets in event analysed using SISCone algorithm.

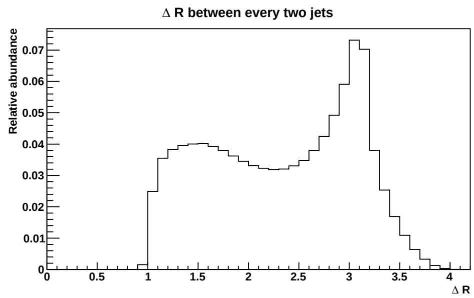

(d) Distance in $\eta - \phi$ space between every two jets in event analysed with FastJet algorithm.

Figure 3.17: Cosine of angle, (a) and (b), and Δ R, (c) and (d), between every two jets in event.

3.2.2 Method for b-tagging in ALICE

From methods presented before, following algorithm was tested.

All jets were reconstructed by standard jet finding algorithm, SISCone or FastJet in case of this work. Subsequently, beauty hadron was identified with help of secondary vertexing algorithm.

Then jets with direction of beauty hadron close enough to jet axis is tagged as beauty jet.

In following sections up to section 3.2.5, where beauty jets are analysed, these are tagged in same manner, but with vertices of beauty hadrons' decays from simulated Monte-Carlo data, rather than vertices reconstructed using secondary vertex algorithms, utilised in section 3.2.5.

3.2.3 Beauty hadrons in jets

As I have in every event at least one pair of beauty flavoured quark and anti-quark and enhanced jet production, production of jets from particles other than these quarks shall be significantly suppressed in data sample. Thus by checking displacement of direction of hadron containing beauty quark from jet axis, i.e. mean value of momenta of particles inside of jets, we get in both cases, FastJet and SISCone, Fig. 3.18b and Fig. 3.18a respectively, significant peak close to 0 in $\eta - \phi$ space. Another peak is seen at the 3.14 value, meaning that closest B-hadron to jets have ϕ-coordinate shifted by 3.14.

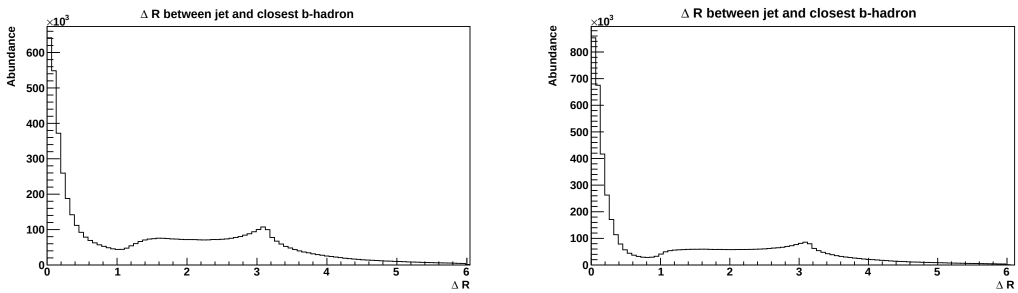

(a) Distance between jet and closest beauty hadron in $\eta - \phi$ space for jets reconstructed with SISCone algorithm.

(b) Distance between jet and closest beauty hadron in $\eta - \phi$ space for jets reconstructed with FastJet algorithm.

Figure 3.18: Distance between jet and closest beauty hadron in $\eta - \phi$ space for SISCone, (a), and FastJet algortihm, (b).

As seen in Fig 3.19b, $\Delta\eta$ distribution for jets with closest beauty hadron in $\Delta R \in \langle 3.14, 3.18 \rangle$, there are 2 distinct peaks relatively close together and significant depression between them at $\Delta\eta = 0$. This indicates that beauty hadrons may be produced in such process, that would not need them to be back-to-back, e.g. final state shower. Also, this case is dominated with $\Delta\phi \approx 3.14$, as seen in Fig. 3.19c, pointing to jet and beauty hadrons to be back-to-back. This behaviour is seen with jets of both algorithms, but in case of SISCone, Fig. 3.19a, two overlapping jets may be easily created and these later merged into one final jet, therefore depression at $\eta \approx 0$ is slightly smaller than that in case of FastJet.

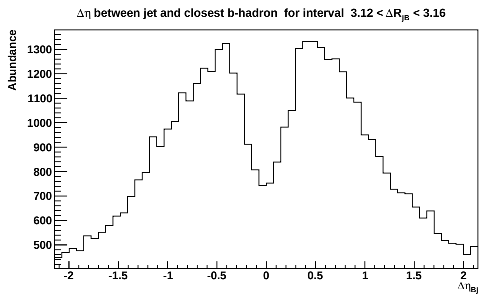

(a) Distribution of $\Delta\eta$ for SISCone algorithm.

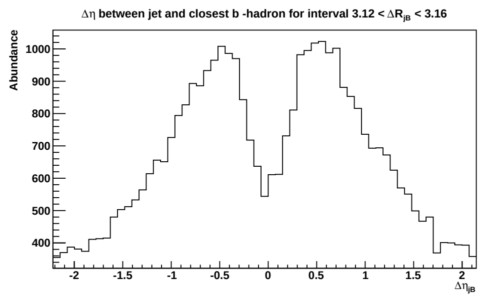

(b) Distribution of $\Delta\eta$ for FastJet algorithm.

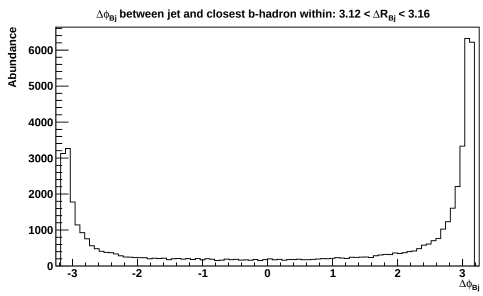

(c) Distribution of $\Delta\phi$ for FastJet algorithm.

Figure 3.19: $\Delta\eta$ and $\Delta\phi$ distributions between jet and closest b-hadron, when distance between them is $\Delta R \in (3.12, 3.16)$.

Energy and mass ratios of closest b-hadrons and jets are shown in Fig. 3.20. In Fig. 3.20a and Fig. 3.20b, are average energy and mass fractions, respectively, in interval $\Delta R \in \langle 0, 0.1 \rangle$. Maxima in this interval are at 0.05 for energy ratio, with ratio slightly more than 1. Maxima of mass ratios are for SISCone at 0.095 and 0.08 for FastJet. This difference is much more significant in the interval $\Delta R \in \langle 0, 1 \rangle$, Fig 3.20d, where minima differ by 0.4 in ΔR. In case of energy ratios, Fig. 3.20c, with increasing ΔR difference between ratios increases, having common minimum at $\Delta R \approx 0.4$.

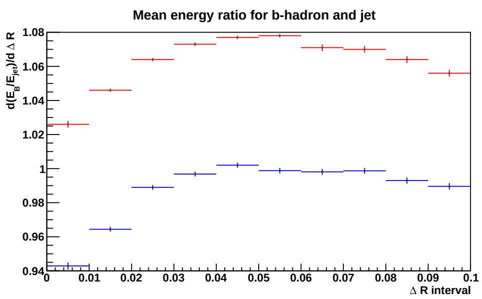

(a) Average energy ratio between closest b-hadron and jet in interval $\Delta R \in \langle 0, 0.1\rangle$.

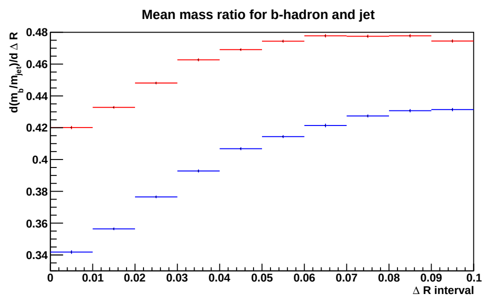

(b) Average invariant mass ratio between closest b-hadron and jet in interval $\Delta R \in \langle 0, 0.1\rangle$.

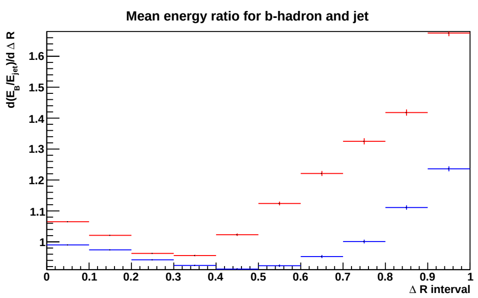

(c) Average energy ratio between closest b-hadron and jet in interval $\Delta R \in \langle 0, 1\rangle$.

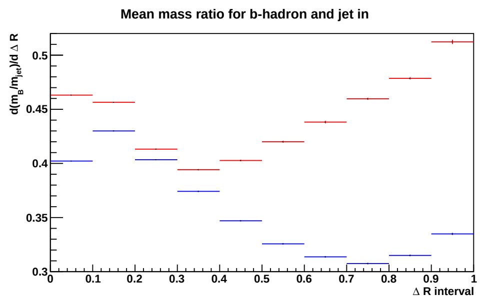

(d) Average mass ratio between closest b-hadron and jet in interval $\Delta R \in \langle 0, 1\rangle$.

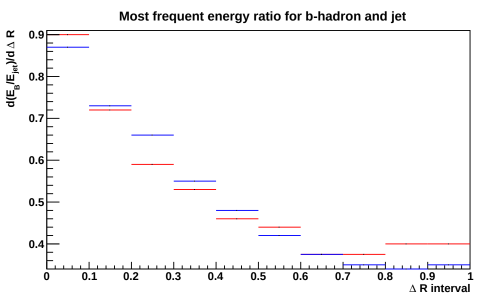

(e) Most frequent energy ratio between closest b-hadron and jet in interval $\Delta R \in \langle 0, 1\rangle$.

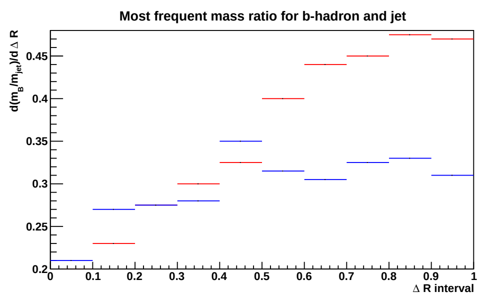

(f) Most frequent mass ratio between closest b-hadron and jet in interval $\Delta R \in \langle 0, 1\rangle$.

Figure 3.20: Energy and mass ratios between closest b-hadron and jet in given ΔR interval, where SISCone jets are drawn with blue and FastJet jets with red lines.

For most frequent, peak, values, difference in energy ratios is small and decreases with increasing ΔR interval. This behaviour differs from average energy ratio from $\Delta R \approx 0.3$. In case of most frequent values of mass ratio, both algorithm show similar behaviour up to $\Delta R \approx 0.5$. From this value on, FastJet algorithm incorporates relatively more energy than SISCone, what reflects also in slightly greater invariant masses.

In general, FastJet reconstructs greater energies and invariant masses with respect to closest b-hadron, than masses and energies in case of SISCone algorithm. Usually, jet is considered b-jet, when beauty hadron is located inside a sub-cone with radius $\Delta R_{jB} \approx 0.3 \div 0.4$, i.e. distance in $\eta - \phi$ space from jet direction must be smaller than this value. From this value we observe start of continual increase in energy and invariant mass fractions.

3.2.4 Particles in jets

In this part of analysis, I am going to focus on distributions of particles in jets. For this purpose, I looked on jet shapes and j_T distribution of particles for jets tagged as b-jets, i.e. jets with closest b-hadron in interval $\Delta R \in \langle 0, 0.4 \rangle$.

Jet shapes

Jet shapes, or differential jet shapes, $\rho(r)$, are distributions of fractional transverse momentum inside a jet as a function of distance from jet axis. Integrated jet shape, $\Psi(R)$, is fraction of total transverse momentum in a cone of radius r to the total transverse momentum carried by jet. Differential jet shape is defined as equation 3.4, where integrated jet shape is defined as $\Psi(r) = \int_0^r \rho(x)dx$.

$$\rho(r) = \frac{d\Psi}{dr} = \frac{1}{N_{jets}} \lim_{\Delta r \to 0} \sum_{jets} \frac{p_T(0, r + \Delta r) - p_T(0, r)}{p_T(0, R)\Delta r} \tag{3.4}$$

Integrated jet shape in analysis is defined by equation 3.5. Integrated jet shapes are by definition equal $\Psi(r = R) = 1$, and by definition $\Psi(r = 0) = 0$.

$$\Psi(r) = \frac{1}{N_{jets}} \sum_{jets} \frac{p_T(0, r)}{p_T(0, R)} \tag{3.5}$$

In Fig. 3.21, differential and integrated jet shapes are shown. These are for jets with closest b-hadron $\Delta R < 0.4$, $\Delta R < 0.2$ and $\Delta R < 0.1$, for all particles inside jet within radius $R = 1$.

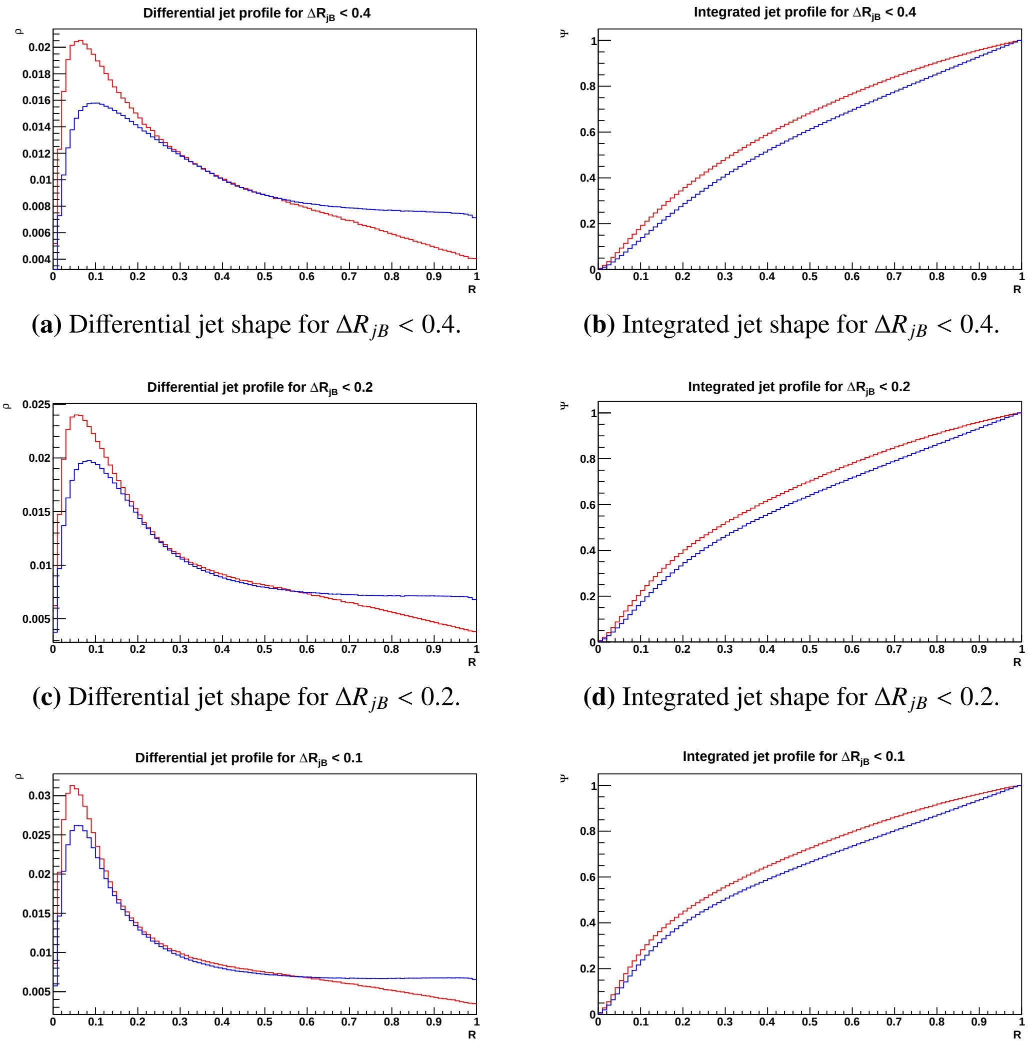

(a) Differential jet shape for $\Delta R_{jB} < 0.4$.
(b) Integrated jet shape for $\Delta R_{jB} < 0.4$.
(c) Differential jet shape for $\Delta R_{jB} < 0.2$.
(d) Integrated jet shape for $\Delta R_{jB} < 0.2$.
(e) Differential jet shape for $\Delta R_{jB} < 0.1$.
(f) Integrated jet shape for $\Delta R_{jB} < 0.1$.

Figure 3.21: Total differential and integrated jet shapes of b-tagged jets, for SISCone algorithm, blue line, and FastJet, red line.

With decreasing minimal distance of jet and closest b-hadron maxima of these distribution increase and are shifted towards jet axis for both SISCone and FastJet algorithm. At greater distances SISCone algorithm produces shallower decrease in distribution, compared to FastJet's steady decrease towards 0. In general only slight variation in p_T distribution is observed with decreasing maximal distance of beauty

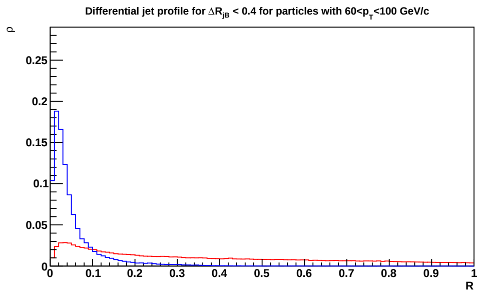

(a) Differential jet shape for particles with $60 < p_T < 100$ GeV/c in b-tagged jets.

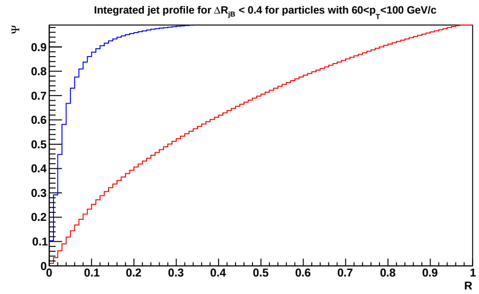

(b) Integrated jet shape for particles with $60 < p_T < 100$ GeV/c in b-tagged jets.

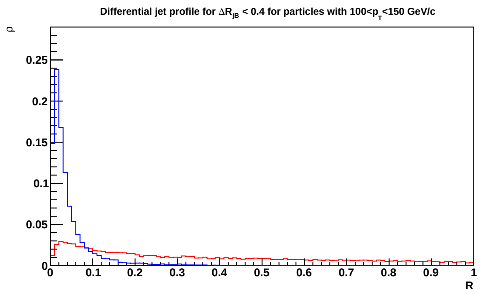

(c) Differential jet shape for particles with $100 < p_T < 150$ GeV/c in b-tagged jets.

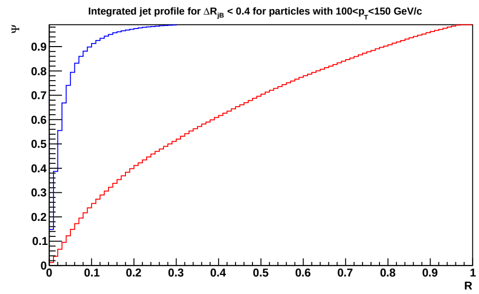

(d) Integrated jet shape for particles with $100 < p_T < 150$ GeV/c in b-tagged jets.

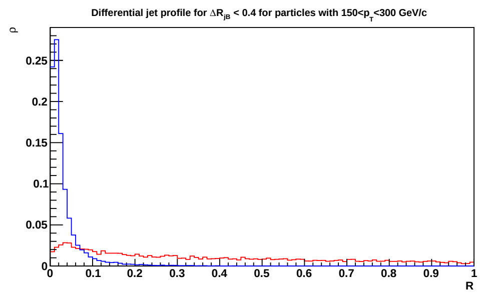

(e) Differential jet shape for particles with $150 < p_T < 300$ GeV/c in b-tagged jets.

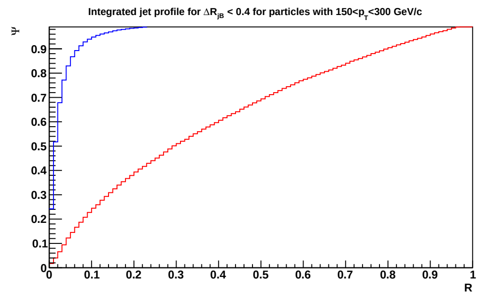

(f) Integrated jet shape for particles with $150 < p_T < 300$ GeV/c in b-tagged jets.

Figure 3.22: Differential and integrated jet shapes of b-tagged jets, i.e. with $\Delta R_{jB} < 0.4$ for given particle p_T bin. Shapes of SISCone jets are drawn with blue line, FastJet jet shapes with red.

hadron from jet axis.

For distance $\Delta R_{jB} < 0.4$, we can observe increasing peak in differential jet shape for SISCone jets, with increasing transverse momenta of particles, Fig. 3.22.

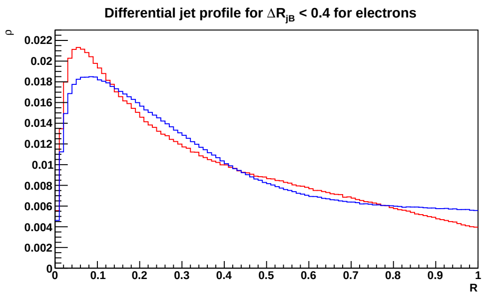

(a) Differential jet shape of electrons for b-tagged jets.

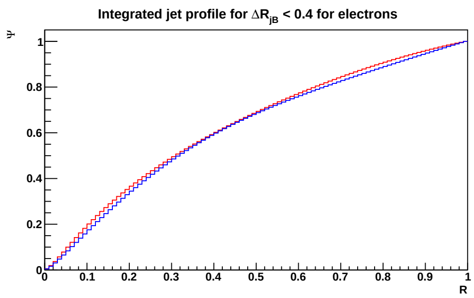

(b) Integrated jet shape of electrons for b-tagged jets.

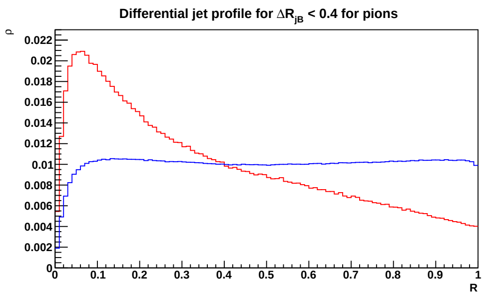

(c) Differential jet shape of pions for b-tagged jets.

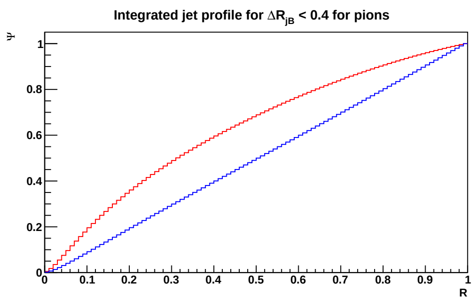

(d) Integrated jet shape of pions for b-tagged jets.

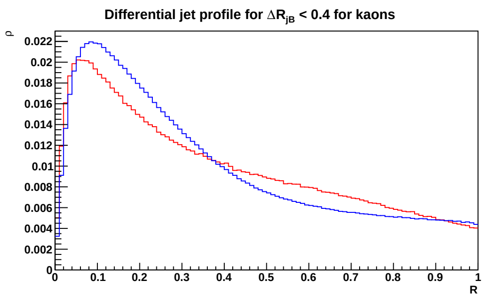

(e) Differential jet shape of kaons for b-tagged jets.

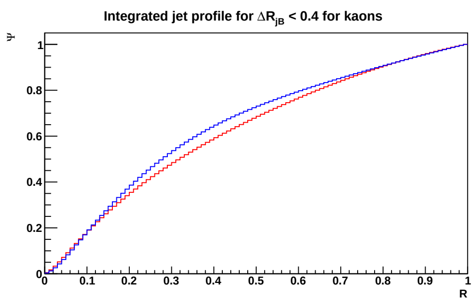

(f) Integrated jet shape of kaons for b-tagged jets.

Figure 3.23: Integrated and differential jet shapes for electrons, (b) and (a), charged pions, (d) and (c), and kaons, (f) and (e), for jets with b-hadron displaced from jet axis maximally to $\Delta R < 0.4$. Shapes of SISCone jets are drawn with blue line, FastJet jet shapes with red.

This reflects in greater slope of integrated jet shapes with increasing p_T bins. These distributions for jets created with FastJet algorithm are different, showing only slight change with increasing particles' transverse momenta, But increase by orders of percent can be seen in $r \approx 0$. In general, these shapes for jets created with FastJet algorithm resemble uniform distribution, mainly for larger radii.

Looking on jets from point of view of different particle types, Fig. 3.23, we see that for electrons and kaons, FastJet and SISCone jets produce similar integrated jets shapes, as well as it is for case of pions in jets reconstructed by FastJet algorithm. But for shapes of pions in SISCone jets, this distribution resembles more an uniform distribution of charged pions.

It is note-worthy to mention, that FastJet's clustering nature may not be as suitable for this type of analysis as it is in case of cone algorithms, because particles reconstructed into jet with FastJet algorithm may be displaced from jet axis by more than R set in reconstruction definition, in section 1.2.2.

j_T

Another method of analysing shape of jet is by studying j_T distribution of particles inside jet. This value represents momentum perpendicular to jet axis as seen in Fig. 3.24 and is given by formula

$$j_T = \sqrt{p_h^2 - \frac{\left(\vec{p_h} \cdot \vec{p_j}\right)^2}{p_j^2}}.$$

Study of jet's internal structure leads to knowledge of quarks' and gluons' fragmentation, leading to jet creation.

j_T distributions for b-jets, jets with beauty hadron displaced within ΔR_{jB} smaller than 0.4, 0.2 and 0.1, are shown in Fig. 3.25a, Fig. 3.25c and Fig. 3.25e, respectively. For these distributions, p_T cut on hadrons is 4 GeV/c. Distributions for hadrons with cut $p_T = 8$ GeV/c are in Fig. 3.25b, Fig. 3.25d and Fig. 3.25f.

From Fig. 3.25, nearly no difference is seen between SISCone jet's j_T structure for hadrons above 4 GeV/c transverse momenta and hadrons with transverse momenta above 8 GeV/c. Further investigation might be necessary for cases with cut on transverse momenta higher than already used.

In case of jets reconstructed with FastJet algorithm slight change is observed in decrease of maxima of j_T distribution. Also decrease of maximal distance of closest beauty hadron from jet reflected into increase of distribution's maximum. In case

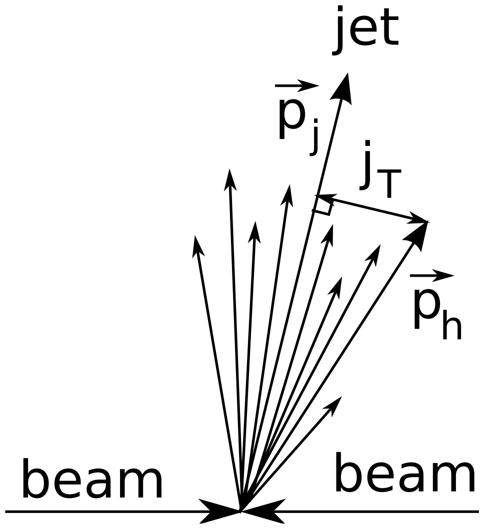

Figure 3.24: Sketch of j_T measured in hadrons of jets, given as transverse component of particle's momentum, arrow labeled with momentum $\vec{p_h}$ from jet axis, here $\vec{p_j}$. This sketch depicts jet created by particles from collision of beam particles, no other particles are shown.

of SISCone, changes are nearly unnoticeable.

Comparing two jet algorithms, we obvious difference is present, in form that j_T is significantly smaller for SISCone algorithm than in case of FastJet, where higher values of j_T are present with comparable probability to probabilities that are dominant in case of SISCone jets.

3.2.5 Secondary vertices

As mentioned in section 1.3, several methods for beauty tagging were suggested. For this analysis, I have used method of secondary vertex reconstruction, focusing on semi-leptonic decay channel of beauty hadrons, mostly mesons. In Fig. 3.2.5 is schematic diagram showing decay of B^- to D^0 and its subsequent decay.

This method utilises relatively long lifetimes mentioned in Tab. 1.2, making it easier to resolve these secondary vertices from vertices created by decay of charm mesons, with $c\tau \sim 100 - 300 \mu m$.

Within this work, following method for identifying beauty hadrons decay vertices was developed. Vertexing starts by finding high-p_T electrons and combining

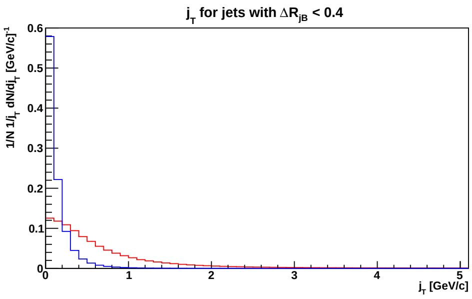

(a) j_T distribution for hadrons with cut p_T = 4 GeV/c and closest b-hadron within $\Delta R_{jB} < 0.4$.

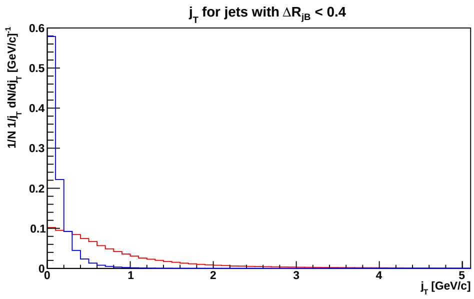

(b) j_T distribution for hadrons with cut p_T = 8 GeV/c and closest b-hadron within $\Delta R_{jB} < 0.4$.

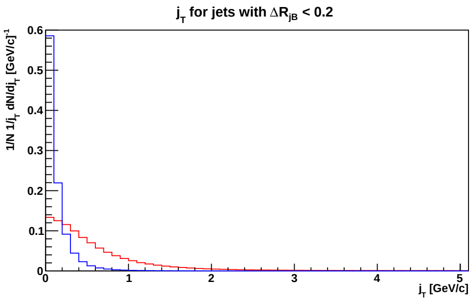

(c) j_T distribution for hadrons with cut p_T = 4 GeV/c and closest b-hadron within $\Delta R_{jB} < 0.2$.

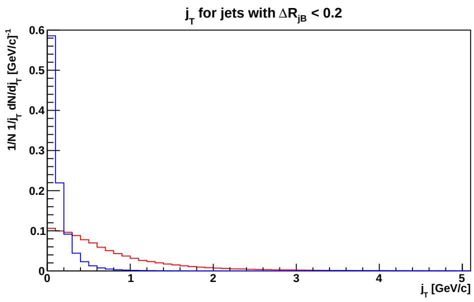

(d) j_T distribution for hadrons with cut p_T = 8 GeV/c and closest b-hadron within $\Delta R_{jB} < 0.2$.

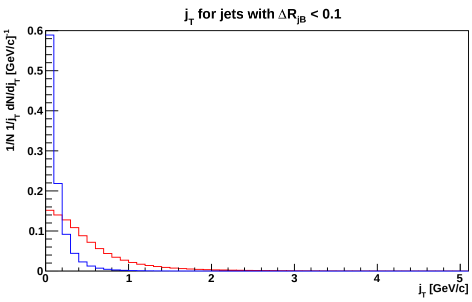

(e) j_T distribution for hadrons with cut p_T = 4 GeV/c and closest b-hadron within $\Delta R_{jB} < 0.1$.

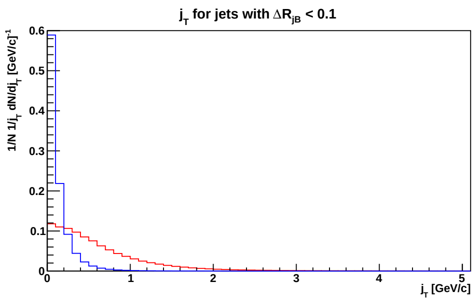

(f) j_T distribution for hadrons with cut p_T = 8 GeV/c and closest b-hadron within $\Delta R_{jB} < 0.1$.

Figure 3.25: j_T distribution for different cut on p_T of hadrons and for different maximal displacements of closest beauty hadron to jet. This is done for both SISCone algorithm, blue line, and FastJet algorithm, red lines.

them with sufficiently close charged particles. An additional condition of $\Delta R < 1.5$ between these reconstructed tracks is imposed, to enhance speed of vertexing algorithm. Apart from small distance of closest approach between tracks, being smaller than 1 mm, or between track candidates and already reconstructed secondary vertex candidate, sufficiently small χ^2 of reconstructed vertex and difference $\Delta\chi^2$ between vertex's χ^2 before and after accepting track as vertex's daughter track is required. For purposes of this analysis, maximal χ^2 of vertex is 100 and difference in this value before and after process of adding track as another daughter shall not exceed $\Delta\chi^2$ equal to 15.

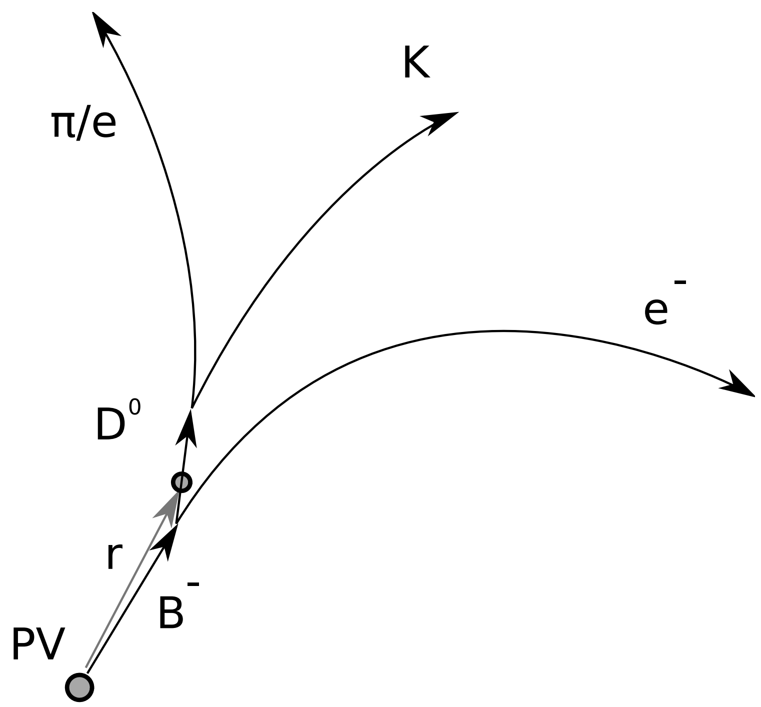

Figure 3.26: Scheme of B^- decay through D^0 meson with it's subsequent decay through K-mesons.

For track selection, 4 ITS hits were required in this analysis. Selected track candidates had to have ITS and TPC refits, transverse impact parameters, distances of closest approach to primary vertex in transverse plane, smaller than 0.5 cm, and distance of closest approach to primary vertex in beam direction smaller than 1 cm. Distance of closest approach to secondary vertex smaller than 0.1 mm. Transverse momenta of electron candidates has to be greater than 1.5 GeV/c, and are checked for possibility of being conversion electron. these electron candidates had to have TPC probability of being electron greater than 80%.

Tracks satisfying these conditions are joined and reconstructed using Kalman filter that is implemented in *AliKFParticle* class in *AliRoot*. Selection of tracks was done on all tracks, not only tracks creating reconstructed jets. Further analysis of reconstruction of vertices from tracks only from jet is needed.

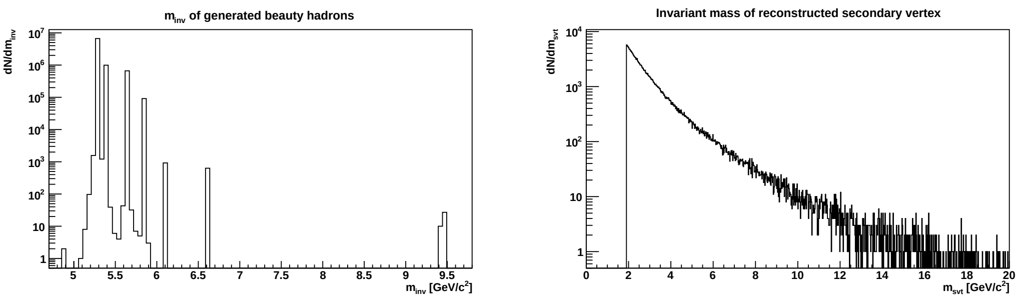

(a) Rest masses of generated beauty hadrons.

(b) Invariant masses of reconstructed secondary vertices, after applying 1.9 GeV/c^2 cut.

Figure 3.27: Invariant masses of generated beauty hadrons, (a), and reconstructed secondary vertices after applying 1.9 GeV/c^2 cut to differentiate decays of charmed mesons, (b).

Subsequently, cuts are applied on invariant mass as beauty hadrons are one of the heaviest hadrons produced, to distinguish D-meson decays, whose energy for are up to 1.9 GeV/c^2. Bottom hadron's mass is from 5.279 GeV/c^2 for B-mesons, up to approximately 9 GeV/c^2 for Υ mesons, occurring in simulated data. For comparison, mass spectra of beauty hadrons are in Fig. 3.27a and reconstructed mass spectra of secondary vertices after applying 1.9 GeV/c^2 cut is in Fig. 3.27b.

In Fig. 3.28a we see number of tracks used in creation of these secondary vertex and in Fig. 3.28b, is energy distribution of secondary vertices obtained from energies of these daughter tracks.

Another observed property of secondary vertices is their displacement from primary vertex, both in transverse plane and in 3 dimensions. Vertices reconstructed in this analysis using tracks chosen by above criteria have their displacements transverse plane plotted in 3.29a. Cut placed on transverse displacement was to be greater than 0.01 mm.

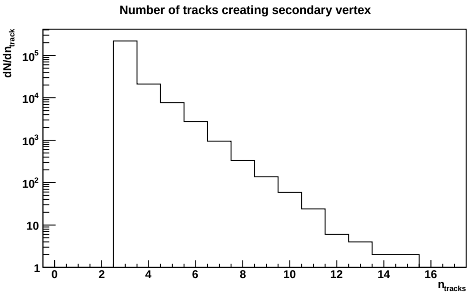

(a) Number of tracks used to reconstruct secondary vertices.

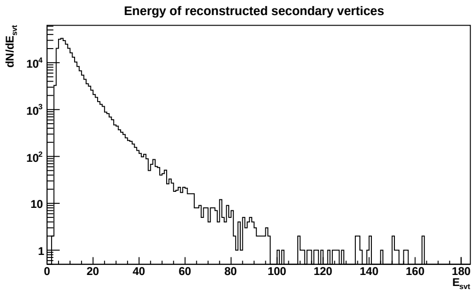

(b) Energy of reconstructed secondary vertices.

Figure 3.28: Number of tracks used to create secondary vertex and energies of these vertices.

Another differentiating variable is cosine of angle between position vector of displacement of secondary vertex from primary vertex and momentum vector of secondary vertex obtained from momenta of its daughter tracks. For this analysis I chose relatively large value of this cosine, being 0.8.

Combining with rejection of vertices from event with no reconstructed jet, number of reconstructed vertices decreased from 251 843 to 103 359.

These vertices have distance from closest jet plotted in Fig. 3.29b, and we observe that in radius of 0.4 in $\eta - \phi$, more than 52% of all these vertices are present. With nearly 17% of all cases, peak in this distribution of distances of secondary vertex from jet in $\eta - \phi$ space is observed at approximately 3.14, corresponding to so called opposite side tagging, when assumption of back-to-back production of beauty quarks is made.

Further enhancement of vertex reconstruction is possible by enhanced electron identification, or by incorporation of other decay channels, by not depending on selected electron.

A study of fake vertex reconstruction has to be carried out, in order to tune above parameters to obtain feasibly small fraction of fake vertices. To increase number of reconstructed beauty hadrons, analysis has to take into account other than semi-electronic decays of these hadrons and comparison with different tagging algorithm should be performed.

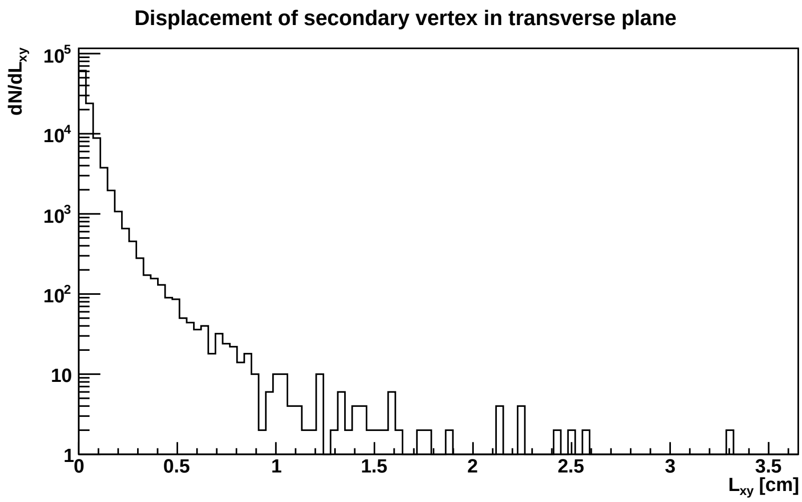

(a) Displacement of secondary vertex from primary vertex in transverse plane.

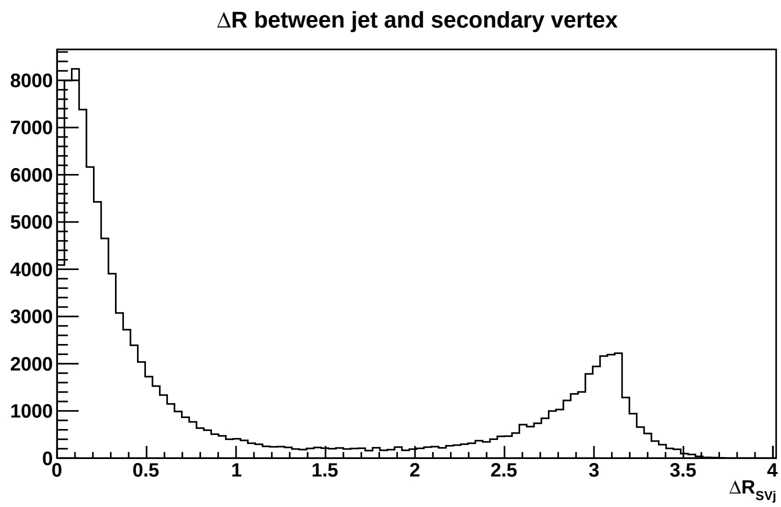

(b) Displacement of secondary vertex from closest jet in $\eta - \phi$.

Figure 3.29: Displacement of secondary vertex from primary vertex in transverse plane, (a), and from jet in $\eta - \phi$, (b).

Summary

In this thesis, detailed analysis of simulated proton-proton collisions at 14 TeV containing b-parton in ALICE detector was performed. Production of beauty hadrons and their properties in these collisions was studied.

The produced jets were reconstructed with both FastJet and SIScone jet algorithms. Both algorithms consistent information on pseudo-rapidity, azimuthal angle distributions and distribution of distances from closest beauty hadron. Varying parameters like R, a geometrical parameter, set for larger values in pp collisions, shall be smaller value, usually up to 4, in case of ion collisions, where higher background is produced and is needed to be subtracted.

Jets reconstructed using these algorithms have slightly different structure, as shown by their jet shapes and j_T distributions. This has to undergo further study, as selection may be improved giving out more precise information about fragmentation of these jets. Also jets containing two quark should be separated and treated distinctly, as they produce different structure than jets created from fragmentation of sole beauty quark.

A method for beauty tagging based on secondary vertexing of semi-electronic decays of beauty hadrons was presented. The variables such as invariant mass or displacement of vertices were proposed to identify such secondary vertices. This method may be chosen not only for tagging of jets, but tagging on general. Additionally, this vertexing may be used to cover not only semi-electronic decays, but decays in general, and shall be compared to other methods, such as probability jet method, that cannot be used for tagging in general. Parameters used in this work, showed possibility of both same-side and opposite-side tagging.

The proposed method has to be evaluated in greater detail, before it can be used in real data analysis.

Bibliography

[1] Aaltonen T. *et al.* *"Measurement of b-jet Shapes in Inclusive Jet Production in $p\bar{p}$ Collisions at $\sqrt{s} = 1.96$ TeV"*, arXiv:0806.1699v4 [hep-ex].

[2] Aamodt, K. *et al.* [ALICE Collaboration], *"Charged-particle multiplicity measurement in proton-proton collisions at $\sqrt{s} = 0.9$ and 2.36 TeV with ALICE at LHC"*, arXiv:1004.3034.

[3] Aamodt K. *et al.* [ALICE Collaboration], *"Charged-particle multiplicity measurement in proton-proton collisions at $\sqrt{s} = 7$ TeV with ALICE at LHC"*, arXiv:1004.3514.

[4] Aamodt K. *et al.* *"First proton-proton collisions at the LHC as observed with the ALICE detector: measurement of the charged-particle pseudorapidity density at $\sqrt{s} = 900$ GeV"*, arXiv: 0911.5430 [hep-ex].

[5] Abazov V. M., *et al.* [The D0 Collaboration], *"b-Jet Identification in the D0 Experiment"*, arXiv:1002.4224 [hep-ex].

[6] Alessandro B., (ed.) et al., *"ALICE: Physics performance report, volume II "*, J.Phys.G32 (2006) 1295.

[7] Blazey G. C., *et al.*, *"Run II jet physics"*, hep-ex/0005012.

[8] Bruna E. [STAR Collaboration], *"Measurements of jet structure and fragmentation from full jet reconstruction in heavy ion collisions at RHIC"*, Nucl. Phys. A **830** (2009) 267C [arXiv:0907.4788 [nucl-ex]].

[9] Cacciari M., *"Recent Progress in Jet Algorithms and Their Impact in Underlying Event Studies"*, arXiv:0906.1598 [hep-ph].

[10] Carminati F., *et al., "ALICE: Physics Performance Report, Volume I "*, J.Phys.G30 (2004) 1517.

[11] Cortese P., *et al., "ALICE electromagnetic calorimeter technical design report"*, CERNLHCC-2008-014 (2008).

[12] Ellis S. D. and Soper D. E., *"Successive combination jet algorithm for hadron collisions"*, Phys. Rev. D **48** (1993) 3160 [arXiv:hep-ph/9305266].

[13] Filimonov K., *"Jets as a probe of dense matter at RHIC"*, J. Phys. G **30**, S919 (2004) [arXiv:nucl-ex/0403060].

[14] Grelli A. and Mischke A., *"Heavy flavour production at LHC"*, arXiv:0909.4769 [hep-ex].

[15] Henry T. [STAR collaboration], *"Full jet reconstruction in $d + Au$ and $p + p$ collisions at RHIC"*, J. Phys. G **30** (2004) S1287, [arXiv:nucl-ex/0403031].

[16] Lister A., *"Measurement of b^- quark Jet Shapes at CDF"*, http://lss.fnal.gov/archive/thesis/fermilab-thesis-2006-08.pdf.

[17] Morsch A., *"Jets in heavy ion collisions at the LHC"*, Acta Phys. Polon. Supp. **1**, 467 (2008).

[18] Neubert M., *"Introduction to B physics"*, arXiv:hep-ph/0001334.

[19] Salam G. P. and Soyez G., *"A practical Seedless Infrared-Safe Cone jet algorithm"*, JHEP **0705** (2007) 086 [arXiv:0704.0292 [hep-ph]].

[20] Salam G. P. and Cacciari M., *"Jet clustering in particle physics, via a dynamic nearest neighbour graph implemented with CGAL"*, http://www.lpthe.jussieu.fr/~salam/repository/docs/kt-cgta-v2.pdf.

[21] Sjöstrand T., Mrenna S. and Skands P., *JHEP05 (2006) 026*.

[22] Qin G. Y., Gale C., Jeon S., Moore G. D. and Ruppert J., *"Jet energy loss and high p_T photon production in hot quark-gluon plasma"*, Nucl. Phys. A **830** (2009) 459C [arXiv:0907.3898 [hep-ph]].

[23] Snider F. D. [CDF Collaboration], *"Vertexing algorithms at hadron colliders"*, Nucl. Instrum. Meth. A **501** (2003) 233.

[24] Sterman G., *"QCD and jets,"* arXiv:hep-ph/0412013.

[25] Wiechula J. [ALICE TPC Collaboration], *"Commissioning and Calibration of the ALICE TPC"*, Nucl. Phys. A **830**, 531C (2009) [arXiv:0907.4257 [nucl-ex]].

[26] http://www.lpthe.jussieu.fr/~salam/fastjet/

[27] http://www.hepforge.org/downloads/siscone/